bioRxiv preprint doi: https://doi.org/10.1101/635961; this version posted May 13, 2019. The copyright holder for this preprint (which was not certified by peer review) is the author/funder. All rights reserved. No reuse allowed without permission.

Detailed profiles of histone modification in male germ line cells of the young and aged mice

Misako Tatehana[1], Ryuichi Kimura[1], Kentaro Mochizuki[1, 2], Noriko Osumi[1]

[1]Department of Developmental Neuroscience, Center for Advanced Research and Translational Medicine (ART), Tohoku University School of Medicine, Sendai, Japan

[2]Department of Medical Genetics, Life Sciences Institute, The University of British Columbia, Vancouver, BC V6T 1Z3, Canada

Keywords: spermatogenesis, aging, histone modifications

bioRxiv preprint doi: https://doi.org/10.1101/635961; this version posted May 13, 2019. The copyright holder for this preprint (which was not certified by peer review) is the author/funder. All rights reserved. No reuse allowed without permission.

Abstract

Human epidemiological studies have shown paternal aging as one of the risks for neurodevelopmental disorders such as autism in offspring. This is modeled in rodents; offspring derived from aged fathers showed behavioral abnormalities. Since we have noticed that some of the behavior traits are not transmitted to the second generation, we are focusing on epigenetic changes that can influence offspring developmental programs. In this study, we qualitatively and semi-quantitatively evaluated histone modification patterns in male germ line cells throughout spermatogenesis based on immunostaining of testes taken from young (3 months) and aged (12 months) old mice. Although localization patterns were not obviously changed between young and aged testes, some histone modification showed differences in their intensity. Among histone modifications that repress gene expression, H3K9me3 was decreased in the male germ line cells in aged testes, while H3K27me2/3 were increased. The intensity of H3K27ac that activates gene expression was relatively low in aged testes. Interestingly, H3K27ac was detected in putative sex chromosomes of round spermatids, while other chromosomes were occupied by a repressive mark H3K27me3. Among other histone modifications that activate gene expression, H3K4me2 was drastically decreased in the male germ line cells in the aged testis. H3K79me3 was contrastingly increased and accumulated on the sex chromosomes at M-phase spermatocytes. Therefore, aging induced alterations in the amount of histone modifications, of which patterns were different in individual histone modifications. Moreover, histone modification seems to be differentially regulated by aging on the sex chromosomes and on others. These findings would help elucidate epigenetic mechanisms underlying influence of paternal aging on offspring's development.

bioRxiv preprint doi: https://doi.org/10.1101/635961; this version posted May 13, 2019. The copyright holder for this preprint (which was not certified by peer review) is the author/funder. All rights reserved. No reuse allowed without permission.

Introduction

Spermatogenesis is a complicated process to ultimately produce sperm, i.e., haploid cells to be fertilized with another haploid cells, i.e., oocytes, and involves dynamic processes, including meiosis of spermatocytes and drastic morphological changes of the germ line cells. Aging is associated with an increased risk of various diseases such as cancer as well as cardiovascular and neurodegenerative diseases [1-3], and in case of spermatogenesis, aging induce reduction of the sperm cell number and decrease in fertility [4, 5]. Paternal aging also affects offspring's health and disease. For example, it is shown from human etiological studies that paternal aging is as one of the risks for neurodevelopmental disorders such as autism spectrum disorder (ASD) in the next generation [6]. There are rodent models showing behavioral abnormalities in offspring derived from aged fathers.

Molecular mechanisms underlying aging include telomere shortening, mitochondrial dysfunction, accumulation and aggregation of misfolded proteins and so forth [7]. In addition, epigenetic alterations have large impact on all these processes, either directly or indirectly [8]. For example, altered sperm DNA methylation due to paternal aging is suggested to contribute to the risk of ASD in offspring [9, 10]. Thus, it is true that aging also affects germ line cells.

Previous studies regarding aging effects on reproductive potential have reported an increased level of DNA damage [11], DNA mutation [12] in sperm derived from aged men and oxidative stress [13] in sperm derived from aged male rats; these factors may cause lower sperm quality and decreased sperm count [14-18]. Recently, epigenetic alteration in sperm and the testis has been reported [19-21], although less attention has been paid on when those alterations occur. Moreover, localization patterns of histone modification in the male germ line cells and their alteration by aging remain unveiled. While most of histone protein is replaced with protamine, some remain on genome regions that are functioning in early developmental stages [22]. Therefore, it might be a clue to understand molecular mechanisms that tune gene regulation after fertilization.

Here we first demonstrated comprehensive intensity profiles of histone modification during murine spermatogenesis. Consistent with a notion that spermatogenesis involves dynamic processes, including meiosis of spermatocytes and drastic morphological changes of the germ line cells, individual epigenetic modifications showed dynamic and distinct localization changes during these processes. Based on these profiles, we further examined influence of aging on histone modifications in each step of spermatogenesis. We found that levels of histone modification were differentially affected by aging during spermatogenesis in the testis. Besides, fluorescent *in situ* hybridization (FISH) analysis

bioRxiv preprint doi: https://doi.org/10.1101/635961; this version posted May 13, 2019. The copyright holder for this preprint (which was not certified by peer review) is the author/funder. All rights reserved. No reuse allowed without permission.

revealed accumulation of H3K79me3 on sex chromosomes. Elucidation of epigenetic mechanisms in aging of the testis would contribute to understanding developmental origin of health and disease of offspring.

bioRxiv preprint doi: https://doi.org/10.1101/635961; this version posted May 13, 2019. The copyright holder for this preprint (which was not certified by peer review) is the author/funder. All rights reserved. No reuse allowed without permission.

Methods

Animals

C57BL/6J mice at 3-months old were purchased from a breeder (Charles River Laboratories, Japan). Some mice were raised up to 5- or 12-months old at Institute for Animal Experimentation Tohoku University Graduate School of Medicine and used for histological and semi-quantitative analyses. All animals were housed in standard cages in a temperature- and humidity-controlled room with a 12-hour light/dark cycle (light on at 8 am), and had free access to standard food and water. All experimental procedures were approved by Ethic Committee for Animal Experiments of Tohoku University Graduate School of Medicine (#2017- MED210), and the animals were treated according to the National Institutes of Health guidance for the care and use of laboratory animals.

Histological analyses of histone modifications

Histological analysis was performed based on a previous our report [23]. Mice were anesthetized with isoflurane and perfused with PBS (pH 7.4) to remove blood. After perfusion, testes were dissected, immersed in 4% PFA in PBS, and cut into half to be post-fixed in 4% PFA overnight at 4˚C. After washing in PBS, the testes were cryoprotected by being immersed in 5 % and 10% sucrose in PBS solution for 1 hour each, 20% sucrose in PBS solution overnight, and embedded in OCT compound (Sakura Finetek, Japan). Frozen sections of the testes were cut at 10 μm on a cryostat (Leica, CM3050).

Next, 0.01M citric acid (pH 6.0) solution was heated up using microwave and kept between 90˚C and 95˚C on a heat plate with gentle stirring. The sections were emerged in the solution for 10 minutes for antigen retrieval. The solution and sections were left to cool down to 40-50˚C, and washed in 1×Tris-based saline containing 0.1% Tween20 (TBST) (pH 7.4), and treated with 3% bovine serum albumin and 0.3% Triton X-100 in PBS solution for blocking. The sections were incubated at 4˚C overnight with the following primary antibodies at 1/500: i.e., rabbit anti-H3K9me3 (ab8898, abcam), rabbit anti-H3K27me2 (ab24684, abcam), rabbit anti-H3K27me3 (07-449, Millipore), rabbit anti-H3K27ac (ab4729, abcam), rabbit anti-H3K79me2 (ab3594, abcam), rabbit anti-H3K79me3 (ab2621, abcam), mouse anti-SYCP3 (ab97672, abcam). Subsequently, either Cy3- or Alexa488-conjugated secondary antibody (1:500) was applied together with 4'6-diamino-2-phenylindole (DAPI), and the sections were incubated at RT for one hour in a humid chamber. After washing in TBST at room temperature, specimens were mounted in Vectashield (Vector Laboratories, H-1200) or ProLong™ Diamond Antifade Mountant (Invitrogen, P36965). Images were captured using a confocal laser-scanning microscope (LSM780, Carl Zeiss, Jena, Germany).

bioRxiv preprint doi: https://doi.org/10.1101/635961; this version posted May 13, 2019. The copyright holder for this preprint (which was not certified by peer review) is the author/funder. All rights reserved. No reuse allowed without permission.

Semi-quantitative analyses of histone modifications

Confocal images of the testis sections were semi-quantitatively analyzed by using ImageJ. SYCP3 signals were used to identify stages of spermatogenesis. A mean intensity of DAPI and each histone modification were measured to normalize histone modification signals by DAPI signal.

DNA Fluorescence in situ hybridization (DNA-FISH) followed by immunofluorescence staining

Antigen retrieval and immunohistochemical staining were performed as described above. Rabbit anti-H3K79me3 (1:500, ab2621, abcam) and Alexa Fluor Plus 647 (1:500, A32728, Invitrogen) were used as primary and secondary antibodies, respectively, and counterstained with DAPI. The sections were mounted in Vectashield. After capturing images using a confocal laser-scanning microscope, cover glasses were removed and the sections were washed in PBS., and immersed in Histo VT One (1:10, 06380-76, Nacalai Tesque) at 90˚C for 25 minutes. After washing in PBS, the sections were immersed in 70% and 100% ethanol, dried in the air, and applied with 10 µl probes for X and Y chromosomes (MXY-10, Chromosome Science Lab). The sections were covered with cover slips and heated at 80˚C on a heat plate (HDB-1N, AS ONE) for 10 minutes. After 15-hour incubation in a humid chamber at 37˚C, the sections were washed in 2×Standard Saline Citrate (SSC) (pH 4.0), and cover slips were removed. The sections were next incubated in 50% formamid-2×SSC at 37˚C for 20 minutes and washed in 1×SSC for 15 minutes at room temperature. The sections were mounted in Vectashield. Images were captured using a confocal laser-scanning microscope.

Statistical analysis

Student's *t*-test was used to determine statistical significance. Values of $*p < 0.05$ and $**p < 0.01$ were considered statistically significant.

bioRxiv preprint doi: https://doi.org/10.1101/635961; this version posted May 13, 2019. The copyright holder for this preprint (which was not certified by peer review) is the author/funder. All rights reserved. No reuse allowed without permission.

Results

1. Morphological profiles showing histone modification patterns during spermatogenesis

Male germ line cells drastically change their morphology during spermatogenesis. Although previous literatures show localization of some histone modifications in these cells [19, 24, 25], comprehensive localization patterns are not fully examined. Here, we first investigated localization of major histone modifications during spermatogenesis according to 12 stages based on a previous report [26]. This staging helped us to morphologically follow each step of spermatogenesis without any marker staining.

(1) Histone modifications that activate gene expression

First, we examined active marks for gene expression, i.e., H3K4me2, H3K4me3, H3K27ac, H3K79me2 and H3K79me3.

(i) H3K4me2

H3K4me2 signal was observed in all stages of seminiferous tubules. At stage VIII in which the earliest meiotic spermatocytes (i.e., preleptotene cells) were located near the periphery of the tubule, a signal of H3K4me2 was detected in the whole nucleus of preleptotene cells, though constitutive heterochromatin did not show the signal (Fig. 1a, arrowhead 1). The signal continued throughout meiosis (Fig. 1a, arrowheads 2-6). In the pachytene cells of stage X, a strong signal was detected on the XY body (Fig. 1a, arrowhead 7). The accumulation of H3K4me2 on the XY body disappeared in the M-phase spermatocytes at stage XII, and only weak signal was observed in the chromosomes (Fig. 1a, arrowhead 8). In round spermatids from stage I to VIII and elongated spermatids at stage X, the signal was widely detected in the nucleus, but not in the chromocenter (constitutive heterochromatin) (Fig. 1a, arrowheads 9-12). Thus, localization of H3K4me2 modification seems to start from preleptotene cells, and to accumulate on the XY body in late pachytene cells. Through spermatogenesis, H3K4me2 was not detected in the chromocenter (Fig. 1b).

(ii) H3K4me3

While H3K4me2 was observed from preleptotene cells (Fig. 1b), H3K4me3 signal was not detected from preleptotene cells to pachytene cells (Fig. 2a, arrowheads 1-7). H3K4me3 was firstly detected in M-phase spermatocytes in stage XII seminiferous tubules (Fig. 2a, arrowhead 8). The signal was broadly distributed on condensed chromosomes (Fig. 2b, arrowhead 8). After meiotic division II, the signal was detected in

bioRxiv preprint doi: https://doi.org/10.1101/635961; this version posted May 13, 2019. The copyright holder for this preprint (which was not certified by peer review) is the author/funder. All rights reserved. No reuse allowed without permission.

round spermatids at stage I to VIII, though there was no signal in the chromocenter (Fig. 2a, arrowheads 9-11). In elongated spermatids, the signal was weak and widely detected in whole nucleus (Fig. 2a, arrowhead 12). Thus, localization of H3K4me3 modification appeared later stage of meiosis, and the signal was weak compare to H3K4me2 modification (Fig. 2b).

(iii) H3K27ac

H3K27ac signal was observed in all stages of seminiferous tubules. At stage VIII in which the earliest meiotic cells (i.e., preleptotene cells) were located near the periphery of the tubule, strong signals of H3K27ac were detected in whole nuclei of preleptotene cells (Fig. 3a, arrowhead 1). While the signal continued throughout meiosis, the intensity dramatically decreased when preleptotene cells differentiated into leptotene cells (Fig. 3a, arrowhead 2-5). In the pachytene cells of stage VIII, a strong signal was detected on the XY body (Fig. 3a, arrowhead 6). The accumulation of H3K27ac on the XY body disappeared in the pachytene cells of stage X and M-phase spermatocytes at stage XII, and only weak signal was observed in the whole nucleus or chromosomes (Fig. 3a, arrowheads 7-8). In round spermatids from stage I to V, the signal was widely detected in the nucleus, especially in the peri-chromocenter (putative sex chromosome) (Fig. 3a, arrowheads 9-10). The strong signal on the peri-chromocenter disappeared in round spermatids of stage VIII (Fig. 3a, arrowhead 11). H3K27ac signal increased again in elongated spermatids, suggesting requirement of H3K27ac for spermiogenesis (Fig. 3a, arrowhead 12). Thus, localization of H3K27ac modification seems to start from preleptotene cells, and to accumulate on the XY body in late pachytene cells and on the putative sex chromosome during early to middle stages of round spermatids (Fig. 3b).

(iv) H3K79me2

In pachytene cells from stage VIII to stage X, the signal was widely detected in the nucleus (Fig. 4a, arrowheads 1 and 2). In M-phase spermatocytes at stage XII, the signal was broadly observed on the condensed chromosomes (Fig. 4a, arrowhead 3). In round spermatids at stage I, a weak signal of H3K79me2 was observed in the most of the nucleus except the chromocenter (Fig. 4a, arrowhead 4). Interestingly, a strong signal of H3K79me2 was observed in the peri-chromocenter (a putative sex chromosome) in round spermatids from stage V to VIII (Fig. 4a, arrowheads 5 and 6), while no signal was observed on the chromocenter itself. In elongated spermatids at stage X, the strong signal on the putative sex chromosome disappeared (Fig. 4a, arrowhead 7). Thus, localization of H3K79me2 modification seems to start from the late pachytene cells, and to accumulate on the putative sex chromosome during most stages of round spermatids (Fig.

bioRxiv preprint doi: https://doi.org/10.1101/635961; this version posted May 13, 2019. The copyright holder for this preprint (which was not certified by peer review) is the author/funder. All rights reserved. No reuse allowed without permission.

4b).

(v) H3K79me3

While H3K79me2 was observed from the late pachytene cells (Fig. 4b), H3K79me3 signal was not detected in any pachytene cells. H3K79me3 was first detected in M-phase spermatocytes in stage XII seminiferous tubules (Fig. 5a, arrowhead 8). Unlike H3K79me2, H3K79me3 signal was not distributed on all condensed chromosomes, but on specific chromosomes (Fig. 5a, arrowhead 8). After meiotic division II, the signal was not detected in round spermatids at stage I (Fig. 5a, arrowhead 9). However, in round spermatids from stage V to VIII, H3K79me3 signal was observed again in the nucleus broadly and strong signal was detected in the peri-chromocenter (a putative sex chromosome) (Fig. 5a, arrowheads 10-11). In elongated spermatids at stage X, the signal was widely observed in the nucleus (Fig. 5a, arrowhead 12). Thus, H3K79me3 modification appeared from the late stage of meiosis, and accumulated on the putative sex chromosome of round spermatids. A specific area of condensed chromosomes showed strong signal of H3K79me3 during M-phase (Fig. 5b).

(2) Histone modifications that inhibit gene expression

Next, we examined repressive marks, H3K9me3, H3K27me2 and H3K27me3.

(i) H3K9me3

H3K9me3 was detected in all cell types examined in this study. Broad nuclear signals were observed from preleptotene cells at stage VIII to pachytene cells at stage V with strong dot signals in the periphery of the nucleus (Fig. 6a, arrowheads 1-5). In pachytene cells at stage VIII and stage X, only dot-like signals were detected (Fig. 6a, arrowheads 6-7). Those dotted signals matched with intense DAPI signals, indicating heterochromatin areas. Consistent with a previous report [27], H3K9me3 exceptionally localized on the sex chromosome of M-phase spermatocytes at stage XII (Fig. 6a, arrowhead 8). In round spermatids at stage I to elongated spermatids at stage X, the signal was detected on the chromocenter and peri-chromocenter (putative sex chromosome) (Fig. 6a, arrowheads 9-12). Thus, localization of H3K9me3 modification seems to start from preleptotene cells, and to accumulate on the sex chromosome in M-phase spermatocytes until late round spermatids (Fig. 6b).

(ii) H3K27me2

bioRxiv preprint doi: https://doi.org/10.1101/635961; this version posted May 13, 2019. The copyright holder for this preprint (which was not certified by peer review) is the author/funder. All rights reserved. No reuse allowed without permission.

H3K27me2 was detected in the nucleus of leptotene cells in stage X to pachytene cells in stage X in a salt-and-pepper manner (Fig. 7a, arrowheads 2-7). In M-phase spermatocytes at stage XII, the signal was broadly observed on all chromosomes (Fig. 7a, arrowhead 8). In round spermatids at stage I, strong dot-like signals were observed on the chromocenter in addition to weak and broad signals in the nucleus (Fig. 7a, arrowhead 9). The dot-like signals were observed until in round spermatids of stage VIII (Fig. 7a, arrowheads 10-11), and disappeared in elongated spermatids at stage X (Fig. 7a, arrowhead 12). Thus, localization of H3K27me2 modification stated from leptotene cells, and accumulated on chromocenter of all stages of round spermatids, though the signal was relatively weak through spermatogenesis (Fig. 7b).

(iii) H3K27me3

H3K27me3 was detected in all cell types examined in this study except preleptotene cells. In leptotene cells at stage X to pachytene cells in stage X, the signal was broadly and slightly detected in the nucleus (Fig. 8a, arrowheads 2-7). In M-phase spermatocytes at stage XII, the signal was widely observed on all chromosomes (Fig. 8a, arrowhead 8). In round spermatids at stage I to elongated spermatids at stage X, strong dot-like signals were observed on the chromocenter in addition to weak and broad signals in the nucleus (Fig. 8a, arrowhead 12), while strong dot-like signals of H3K27me2 disappeared in elongated spermatids at stage X (Fig. 7a, arrowhead 12). Thus, localization of H3K27me3 modification seems to start from leptotene cells, the same timing as H3K27me2, and to accumulate on the chromocenter in early round spermatids (Fig. 8b).

The above localization patterns of histone modifications during spermatogenesis are shown in Table 1. In summary, H3K4me2 was detected in preleptotene cells to elongated spermatids, and H3K27ac was detected in leptotene cells to elongated spermatids. These two modifications were detected at the early stage of spermatogenesis, while other activation markers were detected at the later stage of spermatogenesis. All repressive makers examined in this study were detected at the early stage of spermatogenesis. All activation markers except H3K4me3 showed specific accumulation on XY body in pachytene cells, or a sex chromosome in round spermatids, while all repressive makers were accumulated on the chromocenter (i.e., constitutive heterochromatin). Only H3K9me3 was accumulated on both sex chromosomes and the chromocenter.

2. Semi-quantitative analyses of histone modifications in young and aged testes

bioRxiv preprint doi: https://doi.org/10.1101/635961; this version posted May 13, 2019. The copyright holder for this preprint (which was not certified by peer review) is the author/funder. All rights reserved. No reuse allowed without permission.

We next performed semi-quantified analyses to examine whether intensity of histone modifications are changed in young and aged testes. The signal of histone modification was measured by ImageJ. The intensity of histone modification was normalized by that of DAPI in the nucleus or chromosomes.

(1) Histone modifications that activate gene expression

No difference was observed in localization patterns of H3K4me2/3, H3K27ac, H3K79me2/3, H3K9me3 and H3K27me2/3 in young and aged testes (Fig. 9a, 10a, 11a, 12a, 13a, 14a, 15a and 16a). However, semi-quantitative analyses revealed difference in intensity levels among histone modifications observed.

(i) H3K4me2

Intensity levels were lower in almost all the cells of the aged testis than in the young testis (Fig. 9b). Only in pachytene cells at stage X, there were no statistical differences.

(ii) H3K4me3

Intensity levels were lower in M-phase spermatocytes at stage XII of the aged testis than in the young testis (Fig. 10b). However, higher intensity was detected in stage VIII round spermatids and stage X elongated spermatids in the aged testis. In other cells, there were no statistical differences.

(iii) H3K27ac

Intensity levels were lower in leptotene cells at stage X, pachytene cells at stage V and X of the aged testis than in the young testis (Fig. 11b). However, higher intensity was detected in stage X elongated spermatids in the aged testis. In other cells, there were no statistical differences.

(iv) H3K79me2

Comparing with the young testis, higher intensity was detected in pachytene cells at stage X, round spermatids at stage VIII, and elongated spermatids at stage X (Fig. 12b) of the aged testis. However, other cells showed no difference in the intensity level.

(v) H3K79me3

Higher intensity was detected in M-phase spermatocytes at stage XII of the aged testis than in the young testis, while lower intensity was observed in round spermatids at stage VIII and elongate spermatids at stage X (Fig. 13b).

bioRxiv preprint doi: https://doi.org/10.1101/635961; this version posted May 13, 2019. The copyright holder for this preprint (which was not certified by peer review) is the author/funder. All rights reserved. No reuse allowed without permission.

(2) Histone modifications that inhibit gene expression

(i) H3K9me3

Intensity levels were lower in almost all the cells of the aged testis than in the young testis (Fig. 14b). However, higher intensity was detected in stage V round spermatids in the aged testis. There were no statistical differences in other cell types.

(ii) H3K27me2

Intensity levels were lower in pachytene cells at stage VIII and round spermatids at stage VIII of the aged testis than in the young testis (Fig. 15b). However, other cells showed higher intensity in the aged testis.

(iii) H3K27me3

Similar to the result of H3K27me2, almost stages of cells showed higher intensity in the aged testis (Fig. 16b). In stage X leptotene cells and stage VIII pachytene cells, lower intensity was detected in the aged testis. There were no statistical differences in other cell types.

The above intensity of histone modifications in the young and aged testis is shown in Table 1. In summary, histone modifications were altered by aging and the alteration patterns were different in individual histone modifications. Among the repressive marks, H3K9me3 level was decreased in the aged testis, while H3K27me2 and H3K27me3 level was increased during spermatogenesis. On the other hand, the intensity level of an activation mark, H3K4me2, was drastically decreased in the aged testis during spermatogenesis. Other histone modifications also showed differences at some stages.

4. Accumulation of H3K79me3 on sex chromosomes

As described above, H3K79me3 was detected in M-phase spermatocytes, round spermatids and elongated spermatids. It is previously reported that H3K79me3 accumulates on XY body in late pachytene cells and on a sex chromosome in round spermatids (Ontoso et al. 2014). In this study, H3K79me3 signal was strongly detected on specific chromosomes in M-phase spermatocytes at stage XII (Fig. 17a). Therefore, we suspected that the chromosome on which H3K79me3 accumulated might be sex chromosomes.

To identify the sex chromosome, we established a new protocol by combining

bioRxiv preprint doi: https://doi.org/10.1101/635961; this version posted May 13, 2019. The copyright holder for this preprint (which was not certified by peer review) is the author/funder. All rights reserved. No reuse allowed without permission.

immunostaining together with fluorescence in situ hybridization (FISH) on the same slide. First, immunostaining was performed to detect H3K79me3 signal in M-phase spermatocytes (Fig. 17b). After images were captured using confocal microscopy, FISH was performed using probes that recognize X and Y chromosomes, respectively, followed by capturing FISH images of the same slides to obtain triple signals (Fig. 17c). Signals of H3K79me3, X chromosome and Y chromosome were detected at the same position of M-phase spermatocytes. Finally, we revealed that H3K79me3 was specifically accumulated on the sex chromosomes in M-phase spermatocytes. This result is consistent with other studies that suggest the accumulation of H3K79me3 on the sex chromosomes in late pachytene cells and round spermatids [28].

bioRxiv preprint doi: https://doi.org/10.1101/635961; this version posted May 13, 2019. The copyright holder for this preprint (which was not certified by peer review) is the author/funder. All rights reserved. No reuse allowed without permission.

Discussion

In this study, we revealed transition of histone modification localization during spermatogenesis and alteration caused by aging. Individual histone modifications showed distinct localization patterns and different timing to start expression. Even among the histone modifications that have similar functions showed different localization patterns. Moreover, intensity of histone modifications were altered by aging. Aged testes showed differential increased/decreased signals of histone modifications at different stages. Therefore, responses to aging seem to be different among histone modifications. We also identified a chromosome in which H3K79me3 accumulated in the M-phase spermatocyte. H3K79me3 was accumulated on sex chromosomes in M-phase spermatocytes and round spermatids. Morphologically, it is revealed that not only H3K79me3, but also other histone modifications such as H3K79me2, H3K27ac and H3K9me3 accumulated on putative sex chromosomes or XY body. The intensity of these histone modification specifically accumulated on the putative sex chromosomes or XY body was also altered by aging at some stages. Therefore, epigenetic regulation of histone modifications may be different between sex chromosomes and other chromosomes, which may also be affected by aging.

In the present study, histone modifications that inhibit gene expression showed more drastic changes in the aged testis. At the pachytene stage of meiosis I, genes on sex chromosomes are transcriptionally shut down by meiotic sex chromosome inactivation (MSCI), and reactivated after meiosis [29]. It is reported that H3K9me3 is involved in silencing of sex chromosomes in meiosis and that if there is no enrichment of H3K9me3, remodeling and silencing of sex chromosomes failed and cause germ cell apoptosis [27]. In post-meiotic spermatids, 87% of X-linked genes remain suppressed, while autosomes are largely active [30]. Moreover, spermatids form a distinct post-meiotic sex chromatin (PMSC) area that is enriched with H3K9me3 [30, 31]. Thus, H3K9me3, a repressive mark, has various roles during meiosis and in the post-meiosis phase. In our result, H3K9me3 appeared from preleptotene cells to elongated spermatids, and drastically decreased in the aged testis during meiosis and in most of the stages of round spermatids. It is assumed in the aged testis that failure of correct chromosome segregation during meiosis or leaky expression of X-linked genes might occur in the post-meiotic spermatids even though the male germ line cells safely pass meiosis.

Another repressive mark, H3K27me3, appeared from leptotene cells to elongated spermatids. A study has reported that H3K27ac may act as an antagonist of Polycomb-

bioRxiv preprint doi: https://doi.org/10.1101/635961; this version posted May 13, 2019. The copyright holder for this preprint (which was not certified by peer review) is the author/funder. All rights reserved. No reuse allowed without permission.

mediated silencing through inhibition of H3K27me3 [32]. H3K27ac showed signals in all stages of the male germ line cells examined, especially in preleptotene cells and elongated spermatids. It is very interesting that H3K27ac and H3K27me3 showed exclusive localization in round spermatids; the former was accumulated on the sex chromosome, while H3K27me3 on the chromocenter, a heterochromatin region. Therefore, the absence of H3K27ac (an activation mark) and presence of H3K27me3 (a repressive mark) in the chromocenter may be reasonable in regard with gene regulation. We found that H3K27me3 was dramatically increased in the aged testis, while H3K27ac showed slightly decreased at certain stages. H3K27me3 inhibits transcription by inducing a compact chromatin structure [33, 34]. Thus, gene expression influenced by H3K27me3 might be more repressed in the aged testis.

It is not easy to elucidate the function of histone modification and its alteration by aging. However, progenia models can be used to know aging-induced phenotypes and their underlying mechanisms. Hutchinson-Gilford progeria syndrome (HGPS) patients show premature aging, and cultured cells derived from HGPS patients exhibit an increase of H4K20me3 and a reduction of both H3K9me3 and H3K27me3 [35], i.e., histone modifications inducing heterochromatin regions [36]. Although this result seems to be rather puzzling based on our general knowledge about parallel regulation of H3K9me3 and H4K20me3, it might be considered that heterochromatin regions are decreased in HGPS patients. Indeed, loss of heterochromatin is considered to be one of the mechanisms involved in aging [37, 38]. However, H3K27me2/3 was increased the most of stages in the aged testis. A similar increase of H3K27me3 is observed in quiescent muscle stem cells due to aging [39]. Therefore, it may reasonable to assume that increase/decrease of H3K27me3 may depend on tissues or cell types. One possible reason of these difference can be explained by activities of histone methyltransferases or demethylases, some of which have tissue- or cell line-specific function [40, 41]. In the case of Polycomb-repressive complex 2 (PRC2) that catalyzes the methylation of H3K27, it transcriptionally represses soma-specific genes and facilitates homeostasis and differentiation during mammalian spermatogenesis [42]. This specificity can be associated with different alteration patterns of histone modification in each tissue or cell line. It might be interesting to know whether H3K27me3 is increased by PRC2 and affected to spermatogenesis.

The sex chromosomes seemed to be unique in localization of histone modifications. In this study, we confirmed accumulation of H3K79me3 on the sex chromosomes in spermatocytes at M phase. A similar localization of H3K9me3 has been shown in a previous study [27]. Moreover, H3K27ac was accumulated on XY body and sex

bioRxiv preprint doi: https://doi.org/10.1101/635961; this version posted May 13, 2019. The copyright holder for this preprint (which was not certified by peer review) is the author/funder. All rights reserved. No reuse allowed without permission.

chromosomes in spermatocytes and in round spermatids, respectively. H3K79me2 also showed a signal on the sex chromosomes in round spermatids. We found that intensity of these histone modifications specifically accumulated on the sex chromosomes and/or XY body were also affected by aging at certain stages. What do those results mean?

According to the database collecting risk genes for autism (SFARI at April 9, 2019), X chromosome has 79 risk genes, which is comparable to 90 and 86 risk genes on the larger chromosomes 1 and 2, respectively. It may be reasonable that these three chromosomes have a large number of autism risk genes depending on their size. However, X chromosome has 16 syndromic genes, whereas chromosome 1 and 2 have only four and five, respectively. Enrichment of the autism risk genes, especially syndromic ones, on X chromosome might explain severer symptoms in female patients because X chromosome of father inevitably transmitted only to a daughter. Therefore, more detailed research focusing on target genes of histone modifications that located on X chromosome would be very interesting.

Our results demonstrated aging-related alteration of histone modifications in spermatogenesis, and other reports have also suggested the possibility of the effect of paternal epigenetic factors on offspring's health [43-46]. Currently, however, there is no report describing how the paternal epigenome is actually inherited to offspring. This will be the next important question in regard with the paternal impact on physical conditions of offspring. Although most of histone protein is replaced with protamine during spermatogenesis, some histone modifications in sperm are remained at promoter regions that are known to regulate embryonic development [22]. Further studies are needed to reveal paternal aging impact on epigenetic mechanisms that may cause transgenerational influence on offspring in regard with health and disease.

bioRxiv preprint doi: https://doi.org/10.1101/635961; this version posted May 13, 2019. The copyright holder for this preprint (which was not certified by peer review) is the author/funder. All rights reserved. No reuse allowed without permission.

Acknowledgements

The authors thank Dr. Yasuhisa Matsui for providing insightful comments and assistance, and Ms. Sayaka Makino for animal care. The authors are also grateful to all members of their laboratory for fruitful discussions and advice. This work was supported by KAKENHI (17K19372).

bioRxiv preprint doi: https://doi.org/10.1101/635961; this version posted May 13, 2019. The copyright holder for this preprint (which was not certified by peer review) is the author/funder. All rights reserved. No reuse allowed without permission.

Reference

1. Niccoli T, Partridge L. Ageing as a risk factor for disease. Current biology : CB. 2012;22(17):R741-52. Epub 2012/09/15. doi: 10.1016/j.cub.2012.07.024. PubMed PMID: 22975005.

2. Smetana K, Jr., Lacina L, Szabo P, Dvorankova B, Broz P, Sedo A. Ageing as an Important Risk Factor for Cancer. Anticancer research. 2016;36(10):5009-17. Epub 2016/11/01. doi: 10.21873/anticanres.11069. PubMed PMID: 27798859.

3. Pitt JN, Kaeberlein M. Why is aging conserved and what can we do about it? PLoS biology. 2015;13(4):e1002131. Epub 2015/04/30. doi: 10.1371/journal.pbio.1002131. PubMed PMID: 25923592; PubMed Central PMCID: PMCPmc4414409.

4. Stewart AF, Kim ED. Fertility concerns for the aging male. Urology. 2011;78(3):496-9. Epub 2011/09/03. doi: 10.1016/j.urology.2011.06.010. PubMed PMID: 21884897.

5. Zitzmann M. Effects of age on male fertility. Best practice & research Clinical endocrinology & metabolism. 2013;27(4):617-28. Epub 2013/09/24. doi: 10.1016/j.beem.2013.07.004. PubMed PMID: 24054934.

6. Sandin S, Schendel D, Magnusson P, Hultman C, Suren P, Susser E, et al. Autism risk associated with parental age and with increasing difference in age between the parents. Molecular psychiatry. 2016;21(5):693-700. Epub 2015/06/10. doi: 10.1038/mp.2015.70. PubMed PMID: 26055426; PubMed Central PMCID: PMCPmc5414073.

7. Lopez-Otin C, Blasco MA, Partridge L, Serrano M, Kroemer G. The hallmarks of aging. Cell. 2013;153(6):1194-217. Epub 2013/06/12. doi: 10.1016/j.cell.2013.05.039. PubMed PMID: 23746838; PubMed Central PMCID: PMCPmc3836174.

8. Ashapkin VV, Kutueva LI, Vanyushin BF. Aging as an Epigenetic Phenomenon. Current genomics. 2017;18(5):385-407. Epub 2017/10/31. doi: 10.2174/1389202918666170412112130. PubMed PMID: 29081695; PubMed Central PMCID: PMCPmc5635645.

9. Feinberg JI, Bakulski KM, Jaffe AE, Tryggvadottir R, Brown SC, Goldman LR, et al. Paternal sperm DNA methylation associated with early signs of autism risk in an autism-enriched cohort. International journal of epidemiology. 2015;44(4):1199-210. Epub 2015/04/17. doi: 10.1093/ije/dyv028. PubMed PMID: 25878217; PubMed Central PMCID: PMCPmc4598797.

10. Milekic MH, Xin Y, O'Donnell A, Kumar KK, Bradley-Moore M, Malaspina D, et al. Age-related sperm DNA methylation changes are transmitted to offspring and associated with abnormal behavior and dysregulated gene expression. Molecular psychiatry. 2015;20(8):995-1001. Epub 2014/08/06. doi: 10.1038/mp.2014.84. PubMed PMID: 25092244.

bioRxiv preprint doi: https://doi.org/10.1101/635961; this version posted May 13, 2019. The copyright holder for this preprint (which was not certified by peer review) is the author/funder. All rights reserved. No reuse allowed without permission.

11. Wyrobek AJ, Eskenazi B, Young S, Arnheim N, Tiemann-Boege I, Jabs EW, et al. Advancing age has differential effects on DNA damage, chromatin integrity, gene mutations, and aneuploidies in sperm. Proceedings of the National Academy of Sciences of the United States of America. 2006;103(25):9601-6. Epub 2006/06/13. doi: 10.1073/pnas.0506468103. PubMed PMID: 16766665; PubMed Central PMCID: PMCPmc1480453.

12. Yoon SR, Qin J, Glaser RL, Jabs EW, Wexler NS, Sokol R, et al. The ups and downs of mutation frequencies during aging can account for the Apert syndrome paternal age effect. PLoS genetics. 2009;5(7):e1000558. Epub 2009/07/14. doi: 10.1371/journal.pgen.1000558. PubMed PMID: 19593369; PubMed Central PMCID: PMCPmc2700275.

13. Weir CP, Robaire B. Spermatozoa have decreased antioxidant enzymatic capacity and increased reactive oxygen species production during aging in the Brown Norway rat. Journal of andrology. 2007;28(2):229-40. Epub 2006/10/06. doi: 10.2164/jandrol.106.001362. PubMed PMID: 17021340.

14. Auger J, Kunstmann JM, Czyglik F, Jouannet P. Decline in semen quality among fertile men in Paris during the past 20 years. The New England journal of medicine. 1995;332(5):281-5. Epub 1995/02/02. doi: 10.1056/nejm199502023320501. PubMed PMID: 7816062.

15. Fisch H, Goluboff ET, Olson JH, Feldshuh J, Broder SJ, Barad DH. Semen analyses in 1,283 men from the United States over a 25-year period: no decline in quality. Fertility and sterility. 1996;65(5):1009-14. Epub 1996/05/01. PubMed PMID: 8612826.

16. Neaves WB, Johnson L, Porter JC, Parker CR, Jr., Petty CS. Leydig cell numbers, daily sperm production, and serum gonadotropin levels in aging men. The Journal of clinical endocrinology and metabolism. 1984;59(4):756-63. Epub 1984/10/01. doi: 10.1210/jcem-59-4-756. PubMed PMID: 6434579.

17. Johnson L, Petty CS, Neaves WB. Influence of age on sperm production and testicular weights in men. Journal of reproduction and fertility. 1984;70(1):211-8. Epub 1984/01/01. PubMed PMID: 6694139.

18. Homonnai ZT, Fainman N, David MP, Paz GF. Semen quality and sex hormone pattern of 29 middle aged men. Andrologia. 1982;14(2):164-70. Epub 1982/03/01. PubMed PMID: 6808865.

19. Dottermusch-Heidel C, Klaus ES, Gonzalez NH, Bhushan S, Meinhardt A, Bergmann M, et al. H3K79 methylation directly precedes the histone-to-protamine transition in mammalian spermatids and is sensitive to bacterial infections. Andrology. 2014;2(5):655-65. Epub 2014/08/01. doi: 10.1111/j.2047-2927.2014.00248.x. PubMed PMID: 25079683.

20. Santi D, De Vincentis S, Magnani E, Spaggiari G. Impairment of sperm DNA methylation in male infertility: a meta-analytic study. Andrology. 2017;5(4):695-703. Epub

bioRxiv preprint doi: https://doi.org/10.1101/635961; this version posted May 13, 2019. The copyright holder for this preprint (which was not certified by peer review) is the author/funder. All rights reserved. No reuse allowed without permission.

2017/07/19. doi: 10.1111/andr.12379. PubMed PMID: 28718528.

21. Nasri F, Gharesi-Fard B, Namavar Jahromi B, Farazi-Fard MA, Banaei M, Davari M, et al. Sperm DNA methylation of H19 imprinted gene and male infertility. Andrologia. 2017;49(10). Epub 2017/03/16. doi: 10.1111/and.12766. PubMed PMID: 28295500.

22. Hammoud SS, Nix DA, Zhang H, Purwar J, Carrell DT, Cairns BR. Distinctive chromatin in human sperm packages genes for embryo development. Nature. 2009;460(7254):473-8. Epub 2009/06/16. doi: 10.1038/nature08162. PubMed PMID: 19525931; PubMed Central PMCID: PMCPmc2858064.

23. Kimura R, Yoshizaki K, Osumi N. Dynamic expression patterns of Pax6 during spermatogenesis in the mouse. Journal of anatomy. 2015;227(1):1-9. Epub 2015/06/03. doi: 10.1111/joa.12318. PubMed PMID: 26032914; PubMed Central PMCID: PMCPmc4475354.

24. Xie C, Shen H, Zhang H, Yan J, Liu Y, Yao F, et al. Quantitative proteomics analysis reveals alterations of lysine acetylation in mouse testis in response to heat shock and X-ray exposure. Biochimica et biophysica acta Proteins and proteomics. 2018;1866(3):464-72. Epub 2017/12/03. doi: 10.1016/j.bbapap.2017.11.011. PubMed PMID: 29196234.

25. Zhang L, Wang J, Pan Y, Jin J, Sang J, Huang P, et al. Expression of histone H3 lysine 4 methylation and its demethylases in the developing mouse testis. Cell and tissue research. 2014;358(3):875-83. Epub 2014/09/27. doi: 10.1007/s00441-014-1991-9. PubMed PMID: 25255718.

26. Hess RA, Renato de Franca L. Spermatogenesis and cycle of the seminiferous epithelium. Advances in experimental medicine and biology. 2008;636:1-15. Epub 2009/10/27. doi: 10.1007/978-0-387-09597-4_1. PubMed PMID: 19856159.

27. Hirota T, Blakeley P, Sangrithi MN, Mahadevaiah SK, Encheva V, Snijders AP, et al. SETDB1 Links the Meiotic DNA Damage Response to Sex Chromosome Silencing in Mice. Developmental cell. 2018;47(5):645-59.e6. Epub 2018/11/06. doi: 10.1016/j.devcel.2018.10.004. PubMed PMID: 30393076; PubMed Central PMCID: PMCPmc6286383.

28. Ontoso D, Kauppi L, Keeney S, San-Segundo PA. Dynamics of DOT1L localization and H3K79 methylation during meiotic prophase I in mouse spermatocytes. Chromosoma. 2014;123(1-2):147-64. Epub 2013/10/10. doi: 10.1007/s00412-013-0438-5. PubMed PMID: 24105599; PubMed Central PMCID: PMCPmc3969405.

29. Mueller JL, Mahadevaiah SK, Park PJ, Warburton PE, Page DC, Turner JM. The mouse X chromosome is enriched for multicopy testis genes showing postmeiotic expression. Nature genetics. 2008;40(6):794-9. Epub 2008/05/06. doi: 10.1038/ng.126. PubMed PMID: 18454149; PubMed Central PMCID: PMCPmc2740655.

30. Namekawa SH, Park PJ, Zhang LF, Shima JE, McCarrey JR, Griswold MD, et al. Postmeiotic sex chromatin in the male germline of mice. Current biology : CB. 2006;16(7):660-

bioRxiv preprint doi: https://doi.org/10.1101/635961; this version posted May 13, 2019. The copyright holder for this preprint (which was not certified by peer review) is the author/funder. All rights reserved. No reuse allowed without permission.

7. Epub 2006/04/04. doi: 10.1016/j.cub.2006.01.066. PubMed PMID: 16581510.

31. Turner JM, Mahadevaiah SK, Ellis PJ, Mitchell MJ, Burgoyne PS. Pachytene asynapsis drives meiotic sex chromosome inactivation and leads to substantial postmeiotic repression in spermatids. Developmental cell. 2006;10(4):521-9. Epub 2006/04/04. doi: 10.1016/j.devcel.2006.02.009. PubMed PMID: 16580996.

32. Margueron R, Li G, Sarma K, Blais A, Zavadil J, Woodcock CL, et al. Ezh1 and Ezh2 maintain repressive chromatin through different mechanisms. Molecular cell. 2008;32(4):503-18. Epub 2008/11/26. doi: 10.1016/j.molcel.2008.11.004. PubMed PMID: 19026781; PubMed Central PMCID: PMCPmc3641558.

33. Francis NJ, Kingston RE, Woodcock CL. Chromatin compaction by a polycomb group protein complex. Science (New York, NY). 2004;306(5701):1574-7. Epub 2004/11/30. doi: 10.1126/science.1100576. PubMed PMID: 15567868.

34. Ringrose L, Ehret H, Paro R. Distinct contributions of histone H3 lysine 9 and 27 methylation to locus-specific stability of polycomb complexes. Molecular cell. 2004;16(4):641-53. Epub 2004/11/18. doi: 10.1016/j.molcel.2004.10.015. PubMed PMID: 15546623.

35. Shumaker DK, Dechat T, Kohlmaier A, Adam SA, Bozovsky MR, Erdos MR, et al. Mutant nuclear lamin A leads to progressive alterations of epigenetic control in premature aging. Proceedings of the National Academy of Sciences of the United States of America. 2006;103(23):8703-8. Epub 2006/06/02. doi: 10.1073/pnas.0602569103. PubMed PMID: 16738054; PubMed Central PMCID: PMCPmc1472659.

36. Becker JS, Nicetto D, Zaret KS. H3K9me3-Dependent Heterochromatin: Barrier to Cell Fate Changes. Trends in genetics : TIG. 2016;32(1):29-41. Epub 2015/12/18. doi: 10.1016/j.tig.2015.11.001. PubMed PMID: 26675384; PubMed Central PMCID: PMCPmc4698194.

37. Tsurumi A, Li WX. Global heterochromatin loss: a unifying theory of aging? Epigenetics. 2012;7(7):680-8. Epub 2012/06/01. doi: 10.4161/epi.20540. PubMed PMID: 22647267; PubMed Central PMCID: PMCPmc3414389.

38. Villeponteau B. The heterochromatin loss model of aging. Experimental gerontology. 1997;32(4-5):383-94. Epub 1997/07/01. PubMed PMID: 9315443.

39. Liu L, Cheung TH, Charville GW, Hurgo BM, Leavitt T, Shih J, et al. Chromatin modifications as determinants of muscle stem cell quiescence and chronological aging. Cell reports. 2013;4(1):189-204. Epub 2013/07/03. doi: 10.1016/j.celrep.2013.05.043. PubMed PMID: 23810552; PubMed Central PMCID: PMCPmc4103025.

40. Faralli H, Wang C, Nakka K, Benyoucef A, Sebastian S, Zhuang L, et al. UTX demethylase activity is required for satellite cell-mediated muscle regeneration. The Journal of clinical investigation. 2016;126(4):1555-65. Epub 2016/03/22. doi: 10.1172/jci83239.

bioRxiv preprint doi: https://doi.org/10.1101/635961; this version posted May 13, 2019. The copyright holder for this preprint (which was not certified by peer review) is the author/funder. All rights reserved. No reuse allowed without permission.

PubMed PMID: 26999603; PubMed Central PMCID: PMCPmc4811158.

41. Iwamori N, Iwamori T, Matzuk MM. H3K27 demethylase, JMJD3, regulates fragmentation of spermatogonial cysts. PloS one. 2013;8(8):e72689. Epub 2013/08/24. doi: 10.1371/journal.pone.0072689. PubMed PMID: 23967333; PubMed Central PMCID: PMCPmc3744460.

42. Mu W, Starmer J, Fedoriw AM, Yee D, Magnuson T. Repression of the soma-specific transcriptome by Polycomb-repressive complex 2 promotes male germ cell development. Genes & development. 2014;28(18):2056-69. Epub 2014/09/18. doi: 10.1101/gad.246124.114. PubMed PMID: 25228648; PubMed Central PMCID: PMCPmc4173155.

43. Jenkins TG, James ER, Alonso DF, Hoidal JR, Murphy PJ, Hotaling JM, et al. Cigarette smoking significantly alters sperm DNA methylation patterns. Andrology. 2017;5(6):1089-99. Epub 2017/09/28. doi: 10.1111/andr.12416. PubMed PMID: 28950428; PubMed Central PMCID: PMCPmc5679018.

44. Fullston T, Ohlsson Teague EM, Palmer NO, DeBlasio MJ, Mitchell M, Corbett M, et al. Paternal obesity initiates metabolic disturbances in two generations of mice with incomplete penetrance to the F2 generation and alters the transcriptional profile of testis and sperm microRNA content. FASEB journal : official publication of the Federation of American Societies for Experimental Biology. 2013;27(10):4226-43. Epub 2013/07/13. doi: 10.1096/fj.12-224048. PubMed PMID: 23845863.

45. Gapp K, Jawaid A, Sarkies P, Bohacek J, Pelczar P, Prados J, et al. Implication of sperm RNAs in transgenerational inheritance of the effects of early trauma in mice. Nature neuroscience. 2014;17(5):667-9. Epub 2014/04/15. doi: 10.1038/nn.3695. PubMed PMID: 24728267; PubMed Central PMCID: PMCPmc4333222.

46. McPherson NO, Owens JA, Fullston T, Lane M. Preconception diet or exercise intervention in obese fathers normalizes sperm microRNA profile and metabolic syndrome in female offspring. American journal of physiology Endocrinology and metabolism. 2015;308(9):E805-21. Epub 2015/02/19. doi: 10.1152/ajpendo.00013.2015. PubMed PMID: 25690453.

bioRxiv preprint doi: https://doi.org/10.1101/635961; this version posted May 13, 2019. The copyright holder for this preprint (which was not certified by peer review) is the author/funder. All rights reserved. No reuse allowed without permission.

Figure Legends

Fig. 1 Localization of H3K4me2 in male germ line cells in the young (3 M) testis. (a) Representative confocal images of H3K4me2 (magenta) and SCP3 (green) in the seminiferous epithelium in stages I, V, VIII, X and XII. Nuclei were counterstained with DAPI (blue). The number with arrowhead means as the followings: 1; Preleptotene spermatocyte at stage VIII, 2; Leptotene spermatocyte at stage X, 3; Zygotene spermatocyte at stage XII, 4-7; Pachytene spermatocyte at stage I, V, VIII and X respectively, M; M phase cells at stage XII, 9-11; Round spermatid at stage I, V and VIII respectively, 12; Elongated spermatid at stage X. Scale bar: 20 μm. (b) Magnified images of the cells indicated by arrowheads in (a), and subcellular localization of H3K4me2 in the young testis is shown in magenta in a graphical summary. pL: Preleptotene spermatocyte, L: Leptotene spermatocyte, Z: Zygotene spermatocyte, P: Pachytene spermatocyte, M: M phase, R: Round spermatid, E: Elongated spermatid. Each parenthesis represents the stage of spermatogenesis.

Fig. 2 Localization of H3K4me3 in male germ line cells in the young (3 M) testis. (a) Representative confocal images of H3K4me3 (magenta) and SCP3 (green) in the seminiferous epithelium in stages I, V, VIII, X and XII. Nuclei were counterstained with DAPI (blue). The number with arrowhead means as the followings: 1; Preleptotene spermatocyte at stage VIII, 2; Leptotene spermatocyte at stage X, 3; Zygotene spermatocyte at stage XII, 4-7; Pachytene spermatocyte at stage I, V, VIII and X respectively, M; M phase cells at stage XII, 9-11; Round spermatid at stage I, V and VIII respectively, 12; Elongated spermatid at stage X. Scale bar: 20 μm. (b) Magnified images of the cells indicated by arrowheads in (a), and subcellular localization of H3K4me3 in the young testis is shown in magenta in a graphical summary. pL: Preleptotene spermatocyte, L: Leptotene spermatocyte, Z: Zygotene spermatocyte, P: Pachytene spermatocyte, M: M phase, R: Round spermatid, E: Elongated spermatid. Each parenthesis represents the stage of spermatogenesis.

Fig. 3 Localization of H3K27ac in male germ line cells in the young (3 M) testis. (a) Representative confocal images of H3K27ac (magenta) and SCP3 (green) in the seminiferous epithelium in stages I, V, VIII, X and XII. Nuclei were counterstained with DAPI (blue). The number with arrowhead means as the followings: 1; Preleptotene spermatocyte at stage VIII, 2; Leptotene spermatocyte at stage X, 3; Zygotene spermatocyte at stage XII, 4-7; Pachytene spermatocyte at stage I, V, VIII and X

bioRxiv preprint doi: https://doi.org/10.1101/635961; this version posted May 13, 2019. The copyright holder for this preprint (which was not certified by peer review) is the author/funder. All rights reserved. No reuse allowed without permission.

respectively, M; M phase cells at stage XII, 9-11; Round spermatid at stage I, V and VIII respectively, 12; Elongated spermatid at stage X. Scale bar: 20 μm. (b) Magnified images of the cells indicated by arrowheads in (a), and subcellular localization of H3K27ac in the young testis is shown in magenta in a graphical summary. pL: Preleptotene spermatocyte, L: Leptotene spermatocyte, Z: Zygotene spermatocyte, P: Pachytene spermatocyte, M: M phase, R: Round spermatid, E: Elongated spermatid. Each parenthesis represents the stage of spermatogenesis.

Fig. 4 Localization of H3K79me2 in male germ line cells in the young (3 M) testis. (a) Representative confocal images of H3K79me2 (magenta) and SCP3 (green) in the seminiferous epithelium in stages I, V, VIII, X and XII. Nuclei were counterstained with DAPI (blue). The number with arrowhead means as the followings: 1; Preleptotene spermatocyte at stage VIII, 2; Leptotene spermatocyte at stage X, 3; Zygotene spermatocyte at stage XII, 4-7; Pachytene spermatocyte at stage I, V, VIII and X respectively, M; M phase cells at stage XII, 9-11; Round spermatid at stage I, V and VIII respectively, 12; Elongated spermatid at stage X. Scale bar: 20 μm. (b) Magnified images of the cells indicated by arrowheads in (a), and subcellular localization of H3K79me2 in the young testis is shown in magenta in a graphical summary. pL: Preleptotene spermatocyte, L: Leptotene spermatocyte, Z: Zygotene spermatocyte, P: Pachytene spermatocyte, M: M phase, R: Round spermatid, E: Elongated spermatid. Each parenthesis represents the stage of spermatogenesis.

Fig. 5 Localization of H3K79me3 in male germ line cells in the young (3 M) testis. (a) Representative confocal images of H3K79me3 (magenta) and SCP3 (green) in the seminiferous epithelium in stages I, V, VIII, X and XII. Nuclei were counterstained with DAPI (blue). The number with arrowhead means as the followings: 1; Preleptotene spermatocyte at stage VIII, 2; Leptotene spermatocyte at stage X, 3; Zygotene spermatocyte at stage XII, 4-7; Pachytene spermatocyte at stage I, V, VIII and X respectively, M; M phase cells at stage XII, 9-11; Round spermatid at stage I, V and VIII respectively, 12; Elongated spermatid at stage X. Scale bar: 20 μm. (b) Magnified images of the cells indicated by arrowheads in (a), and subcellular localization of H3K79me3 in the young testis is shown in magenta in a graphical summary. pL: Preleptotene spermatocyte, L: Leptotene spermatocyte, Z: Zygotene spermatocyte, P: Pachytene spermatocyte, M: M phase, R: Round spermatid, E: Elongated spermatid. Each parenthesis represents the stage of spermatogenesis.

bioRxiv preprint doi: https://doi.org/10.1101/635961; this version posted May 13, 2019. The copyright holder for this preprint (which was not certified by peer review) is the author/funder. All rights reserved. No reuse allowed without permission.

Fig.6 Localization of H3K9me3 in male germ line cells in the young (3 M) testis. (a) Representative confocal images of H3K9me3 (magenta) and SCP3 (green) in the seminiferous epithelium in stages I, V, VIII, X and XII. Nuclei were counterstained with DAPI (blue). The number with arrowhead means as the followings: 1; Preleptotene spermatocyte at stage VIII, 2; Leptotene spermatocyte at stage X, 3; Zygotene spermatocyte at stage XII, 4-7; Pachytene spermatocyte at stage I, V, VIII and X respectively, M; M phase cells at stage XII, 9-11; Round spermatid at stage I, V and VIII respectively, 12; Elongated spermatid at stage X. Scale bar: 20 μm. (b) Magnified images of the cells indicated by arrowheads in (a), and subcellular localization of H3K9me3 in the young testis is shown in magenta in a graphical summary. pL: Preleptotene spermatocyte, L: Leptotene spermatocyte, Z: Zygotene spermatocyte, P: Pachytene spermatocyte, M: M phase, R: Round spermatid, E: Elongated spermatid. Each parenthesis represents the stage of spermatogenesis.

Fig. 7 Localization of H3K27me2 in male germ line cells in the young (3 M) testis. (a) Representative confocal images of H3K27me2 (magenta) and SCP3 (green) in the seminiferous epithelium in stages I, V, VIII, X and XII. Nuclei were counterstained with DAPI (blue). The number with arrowhead means as the followings: 1; Preleptotene spermatocyte at stage VIII, 2; Leptotene spermatocyte at stage X, 3; Zygotene spermatocyte at stage XII, 4-7; Pachytene spermatocyte at stage I, V, VIII and X respectively, M; M phase cells at stage XII, 9-11; Round spermatid at stage I, V and VIII respectively, 12; Elongated spermatid at stage X. Scale bar: 20 μm. (b) Magnified images of the cells indicated by arrowheads in (a), and subcellular localization of H3K27me2 in the young testis is shown in magenta in a graphical summary. pL: Preleptotene spermatocyte, L: Leptotene spermatocyte, Z: Zygotene spermatocyte, P: Pachytene spermatocyte, M: M phase, R: Round spermatid, E: Elongated spermatid. Each parenthesis represents the stage of spermatogenesis.

Fig. 8 Localization of H3K27me3 in male germ line cells in the young (3 M) testis. (a) Representative confocal images of H3K27me3 (magenta) and SCP3 (green) in the seminiferous epithelium in stages I, V, VIII, X and XII. Nuclei were counterstained with DAPI (blue). The number with arrowhead means as the followings: 1; Preleptotene spermatocyte at stage VIII, 2; Leptotene spermatocyte at stage X, 3; Zygotene spermatocyte at stage XII, 4-7; Pachytene spermatocyte at stage I, V, VIII and X respectively, M; M phase cells at stage XII, 9-11; Round spermatid at stage I, V and VIII respectively, 12; Elongated spermatid at stage X. Scale bar: 20 μm. (b) Magnified

bioRxiv preprint doi: https://doi.org/10.1101/635961; this version posted May 13, 2019. The copyright holder for this preprint (which was not certified by peer review) is the author/funder. All rights reserved. No reuse allowed without permission.

images of the cells indicated by arrowheads in (a), and subcellular localization of H3K27me3 in the young testis is shown in magenta in a graphical summary. pL: Preleptotene spermatocyte, L: Leptotene spermatocyte, Z: Zygotene spermatocyte, P: Pachytene spermatocyte, M: M phase, R: Round spermatid, E: Elongated spermatid. Each parenthesis represents the stage of spermatogenesis.

Fig. 9 Comparison of localization patterns and intensity of H3K4me2 in male germ line cells in young (3M) and aged (12M) testes. (a) Representative confocal images of H3K4me2 (magenta) in male germ line cells in young and aged testes. Nuclei were counterstained with DAPI (blue). Summarized illustration showing subcellular localization of H3K4me2 (magenta) in male germ line cells in young and aged testes. The number means as the followings: 1; Preleptotene spermatocyte at stage VIII, 2; Leptotene spermatocyte at stage X, 3; Zygotene spermatocyte at stage XII, 4-7; Pachytene spermatocyte at stage I, V, VIII and X respectively, M; M phase cells at stage XII, 9-11; Round spermatid at stage I, V and VIII respectively, 12; Elongated spermatid at stage X. (b) Semi-quantitative analysis of H3K4me2 in male germ line cells in young and aged testes. Black bars show relative intensity of aged cells against young ones (**$p < 0.01$, *$p < 0.05$, n.d., not detected). The red and blue lines mean 20% increased and decrease to the young testis, respectively. pL: Preleptotene spermatocyte, L: Leptotene spermatocyte, Z: Zygotene spermatocyte, P: Pachytene spermatocyte, M: M phase, R: Round spermatid, E: Elongated spermatid. Each parenthesis represents the stage of spermatogenesis.

Fig. 10 Comparison of localization patterns and intensity of H3K4me3 in male germ line cells in young (3M) and aged (12M) testes. (a) Representative confocal images of H3K4me3 (magenta) in male germ line cells in young and aged testes. Nuclei were counterstained with DAPI (blue). Summarized illustration showing subcellular localization of H3K4me3 (magenta) in male germ line cells in young and aged testes. The number means as the followings: 1; Preleptotene spermatocyte at stage VIII, 2; Leptotene spermatocyte at stage X, 3; Zygotene spermatocyte at stage XII, 4-7; Pachytene spermatocyte at stage I, V, VIII and X respectively, M; M phase cells at stage XII, 9-11; Round spermatid at stage I, V and VIII respectively, 12; Elongated spermatid at stage X. (b) Semi-quantitative analysis of H3K4me3 in male germ line cells in young and aged testes. Black bars show relative intensity of aged cells against young ones (**$p < 0.01$, *$p < 0.05$, n.d., not detected). The red and blue lines mean 20% increased and decrease to the young testis, respectively. pL: Preleptotene spermatocyte, L: Leptotene

bioRxiv preprint doi: https://doi.org/10.1101/635961; this version posted May 13, 2019. The copyright holder for this preprint (which was not certified by peer review) is the author/funder. All rights reserved. No reuse allowed without permission.

spermatocyte, Z: Zygotene spermatocyte, P: Pachytene spermatocyte, M: M phase, R: Round spermatid, E: Elongated spermatid. Each parenthesis represents the stage of spermatogenesis.

Fig. 11 Comparison of localization patterns and intensity of H3K27ac in male germ line cells in young (3M) and aged (12M) testes. (a) Representative confocal images of H3K27ac (magenta) in male germ line cells in young and aged testes. Nuclei were counterstained with DAPI (blue). Summarized illustration showing subcellular localization of H3K27ac (magenta) in male germ line cells in young and aged testes. The number means as the followings: 1; Preleptotene spermatocyte at stage VIII, 2; Leptotene spermatocyte at stage X, 3; Zygotene spermatocyte at stage XII, 4-7; Pachytene spermatocyte at stage I, V, VIII and X respectively, M; M phase cells at stage XII, 9-11; Round spermatid at stage I, V and VIII respectively, 12; Elongated spermatid at stage X. (b) Semi-quantitative analysis of H3K27ac in male germ line cells in young and aged testes. Black bars show relative intensity of aged cells against young ones (**$p < 0.01$, *$p < 0.05$, n.d., not detected). The red and blue lines mean 20% increased and decrease to the young testis, respectively. pL: Preleptotene spermatocyte, L: Leptotene spermatocyte, Z: Zygotene spermatocyte, P: Pachytene spermatocyte, M: M phase, R: Round spermatid, E: Elongated spermatid. Each parenthesis represents the stage of spermatogenesis.

Fig. 12 Comparison of localization patterns and intensity of H3K79me2 in male germ line cells in young (3M) and aged (12M) testes. (a) Representative confocal images of H3K79me2 (magenta) in male germ line cells in young and aged testes. Nuclei were counterstained with DAPI (blue). Summarized illustration showing subcellular localization of H3K79me2 (magenta) in male germ line cells in young and aged testes. The number means as the followings: 1; Preleptotene spermatocyte at stage VIII, 2; Leptotene spermatocyte at stage X, 3; Zygotene spermatocyte at stage XII, 4-7; Pachytene spermatocyte at stage I, V, VIII and X respectively, M; M phase cells at stage XII, 9-11; Round spermatid at stage I, V and VIII respectively, 12; Elongated spermatid at stage X. (b) Semi-quantitative analysis of H3K79me2 in male germ line cells in young and aged testes. Black bars show relative intensity of aged cells against young ones (**$p < 0.01$, *$p < 0.05$, n.d., not detected). The red and blue lines mean 20% increased and decrease to the young testis, respectively. pL: Preleptotene spermatocyte, L: Leptotene spermatocyte, Z: Zygotene spermatocyte, P: Pachytene spermatocyte, M:

bioRxiv preprint doi: https://doi.org/10.1101/635961; this version posted May 13, 2019. The copyright holder for this preprint (which was not certified by peer review) is the author/funder. All rights reserved. No reuse allowed without permission.

M phase, R: Round spermatid, E: Elongated spermatid. Each parenthesis represents the stage of spermatogenesis.

Fig. 13 Comparison of localization patterns and intensity of H3K79me3 in male germ line cells in young (3M) and aged (12M) testes. (a) Representative confocal images of H3K79me3 (magenta) in male germ line cells in young and aged testes. Nuclei were counterstained with DAPI (blue). Summarized illustration showing subcellular localization of H3K79me3 (magenta) in male germ line cells in young and aged testes. The number means as the followings: 1; Preleptotene spermatocyte at stage VIII, 2; Leptotene spermatocyte at stage X, 3; Zygotene spermatocyte at stage XII, 4-7; Pachytene spermatocyte at stage I, V, VIII and X respectively, M; M phase cells at stage XII, 9-11; Round spermatid at stage I, V and VIII respectively, 12; Elongated spermatid at stage X. (b) Semi-quantitative analysis of H3K79me3 in male germ line cells in young and aged testes. Black bars show relative intensity of aged cells against young ones (**$p < 0.01$, *$p < 0.05$, n.d., not detected). The red and blue lines mean 20% increased and decrease to the young testis, respectively pL: Preleptotene spermatocyte, L: Leptotene spermatocyte, Z: Zygotene spermatocyte, P: Pachytene spermatocyte, M: M phase, R: Round spermatid, E: Elongated spermatid. Each parenthesis represents the stage of spermatogenesis.

Fig. 14 Comparison of localization patterns and intensity of H3K9me3 in male germ line cells in young (3M) and aged (12M) testes. (a) Representative confocal images of H3K9me3 (magenta) in male germ line cells in young and aged testes. Nuclei were counterstained with DAPI (blue). Summarized illustration showing subcellular localization of H3K9me3 (magenta) in male germ line cells in young and aged testes. The number means as the followings: 1; Preleptotene spermatocyte at stage VIII, 2; Leptotene spermatocyte at stage X, 3; Zygotene spermatocyte at stage XII, 4-7; Pachytene spermatocyte at stage I, V, VIII and X respectively, M; M phase cells at stage XII, 9-11; Round spermatid at stage I, V and VIII respectively, 12; Elongated spermatid at stage X. (b) Semi-quantitative analysis of H3K9me3 in male germ line cells in young and aged testes. Black bars show relative intensity of aged cells against young ones (**$p < 0.01$, *$p < 0.05$, n.d., not detected). The red and blue lines mean 20% increased and decrease to the young testis, respectively pL: Preleptotene spermatocyte, L: Leptotene spermatocyte, Z: Zygotene spermatocyte, P: Pachytene spermatocyte, M: M phase, R: Round spermatid, E: Elongated spermatid. Each parenthesis represents the stage of spermatogenesis.

bioRxiv preprint doi: https://doi.org/10.1101/635961; this version posted May 13, 2019. The copyright holder for this preprint (which was not certified by peer review) is the author/funder. All rights reserved. No reuse allowed without permission.

Fig. 15 Comparison of localization patterns and intensity of H3K27me2 in male germ line cells in young (3M) and aged (12M) testes. (a) Representative confocal images of H3K27me2 (magenta) in male germ line cells in young and aged testes. Nuclei were counterstained with DAPI (blue). Summarized illustration showing subcellular localization of H3K27me2 (magenta) in male germ line cells in young and aged testes. The number means as the followings: 1; Preleptotene spermatocyte at stage VIII, 2; Leptotene spermatocyte at stage X, 3; Zygotene spermatocyte at stage XII, 4-7; Pachytene spermatocyte at stage I, V, VIII and X respectively, M; M phase cells at stage XII, 9-11; Round spermatid at stage I, V and VIII respectively, 12; Elongated spermatid at stage X. (b) Semi-quantitative analysis of H3K27me2 in male germ line cells in young and aged testes. Black bars show relative intensity of aged cells against young ones (**$p < 0.01$, *$p < 0.05$, n.d., not detected). The red and blue lines mean 20% increased and decrease to the young testis, respectively. pL: Preleptotene spermatocyte, L: Leptotene spermatocyte, Z: Zygotene spermatocyte, P: Pachytene spermatocyte, M: M phase, R: Round spermatid, E: Elongated spermatid. Each parenthesis represents the stage of spermatogenesis.

Fig. 16 Comparison of localization patterns and intensity of H3K27me3 in male germ line cells in young (3M) and aged (12M) testes. (a) Representative confocal images of H3K27me3 (magenta) in male germ line cells in young and aged testes. Nuclei were counterstained with DAPI (blue). Summarized illustration showing subcellular localization of H3K27me3 (magenta) in male germ line cells in young and aged testes. The number means as the followings: 1; Preleptotene spermatocyte at stage VIII, 2; Leptotene spermatocyte at stage X, 3; Zygotene spermatocyte at stage XII, 4-7; Pachytene spermatocyte at stage I, V, VIII and X respectively, M; M phase cells at stage XII, 9-11; Round spermatid at stage I, V and VIII respectively, 12; Elongated spermatid at stage X. (b) Semi-quantitative analysis of H3K27me3 in male germ line cells in young and aged testes. Black bars show relative intensity of aged cells against young ones (**$p < 0.01$, *$p < 0.05$, n.d., not detected). The red and blue lines mean 20% increased and decrease to the young testis, respectively. pL: Preleptotene spermatocyte, L: Leptotene spermatocyte, Z: Zygotene spermatocyte, P: Pachytene spermatocyte, M: M phase, R: Round spermatid, E: Elongated spermatid. Each parenthesis represents the stage of spermatogenesis.

bioRxiv preprint doi: https://doi.org/10.1101/635961; this version posted May 13, 2019. The copyright holder for this preprint (which was not certified by peer review) is the author/funder. All rights reserved. No reuse allowed without permission.

Fig. 17 H3K79me3 localization on sex chromosomes in the spermatocyte at M phase. (a) Summarized illustration showing subcellular localization of H3K79me3 (magenta). Lower panels show representative confocal images of H3K79me3 (magenta) and α-tubulin (green) in M phase cells (red square in the summarized illustration) in young and aged testes. Nuclei were counterstained with DAPI (blue). Magnified images of the cells indicated with numbers are shown in the box. (b) Representative confocal images of H3K79me3 (magenta) in M phase cells. Nuclei were counterstained with DAPI (blue). M phase cells are indicated with dotted line and arrowheads. (c) Representative images of FISH showing X (red) and Y (green) chromosomes in M phase cells on the same section as (b). Nuclei were counterstained with Hoechst (blue). The same M phase cells as (b) are indicated with dotted lines and arrowheads.

		pL(VIII)	L (X)	Z(XII)	P(I)	P(V)	P(VIII)	P(X)	M(XII)	R(I)	R(V)	R(VIII)	E(X)	Specific note
H3K4me2	Young	++++	++++	+++	+++	+++	++	++	+++	+++	++++	+++	+++	
	Aged	+++	+++	++	++	++	+	++	++	++	+++	++	++	
H3K4me3	Young	-	-	-	-	-	-	-	++	++	++	++	++	
	Aged	-	-	-	-	-	-	-	+	++	++	+++	+++	
H3K27ac	Young	++++	++	++	+++	+++	+++	+++	++	++	++	++	++++	Accumulation on XY body and sex chromosomes
	Aged	++++	+	++	+++	++	+++	++	++	++	++	++	+++++	
H3K79me2	Young	-	-	-	-	-	++	++	++	++	++	+++	+++	Accumulation on sex chromosomes
	Aged	-	-	-	-	-	++	+++	++	++	++	++++	++++	
H3K79me3	Young	-	-	-	-	-	-	-	++	-	++	++	++	Accumulation on sex chromosomes
	Aged	-	-	-	-	-	-	-	+++	-	++	+	+	
H3K9me3	Young	++	++	++	++	++	++	++	++	++	+++	++++	++++	Accumulation on sex chromosomes and heterochromatin
	Aged	+	+	+	+	+	+	+	++	+	++++	+++	++++	
H3K27me2	Young	-	+++	++	++	+++	+++	+++	++	++	+++	++	+++	Accumulation on heterochromatin
	Aged	-	++++	+++	+++	++++	++	++++	+++	+++	++++	+	++++	
H3K27me3	Young	-	++	++	++	++	++	++	+++	+++	+++	+++	+++	Accumulation on heterochromatin
	Aged	-	+	+++	+++	+++	+++	+	+++	++++	++++	+++	+++	

Table 1 Summarized expression levels of histone modifications during spermatogenesis and their alteration by aging. Expression levels of histone modifications that activate (red) and inhibit (blue) gene expression are shown. Each expression level is indicated in + to +++++. Specific localization or accumulation is described as specific notes.

Fig. 1

a

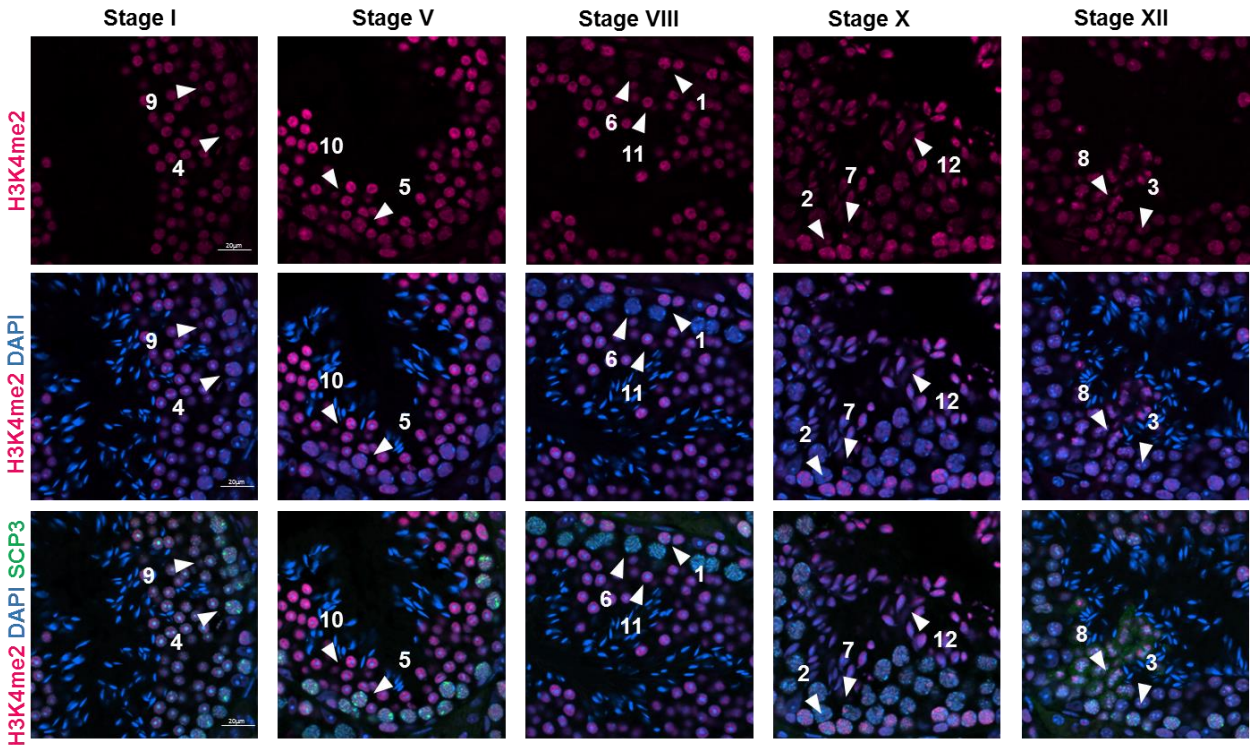

b

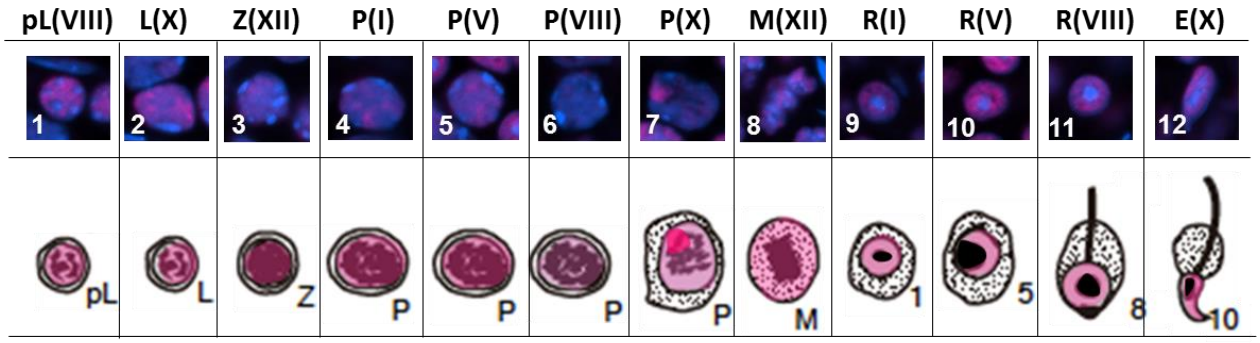

(Modified from Hess & de Franca, 2008)

Fig. 2

a

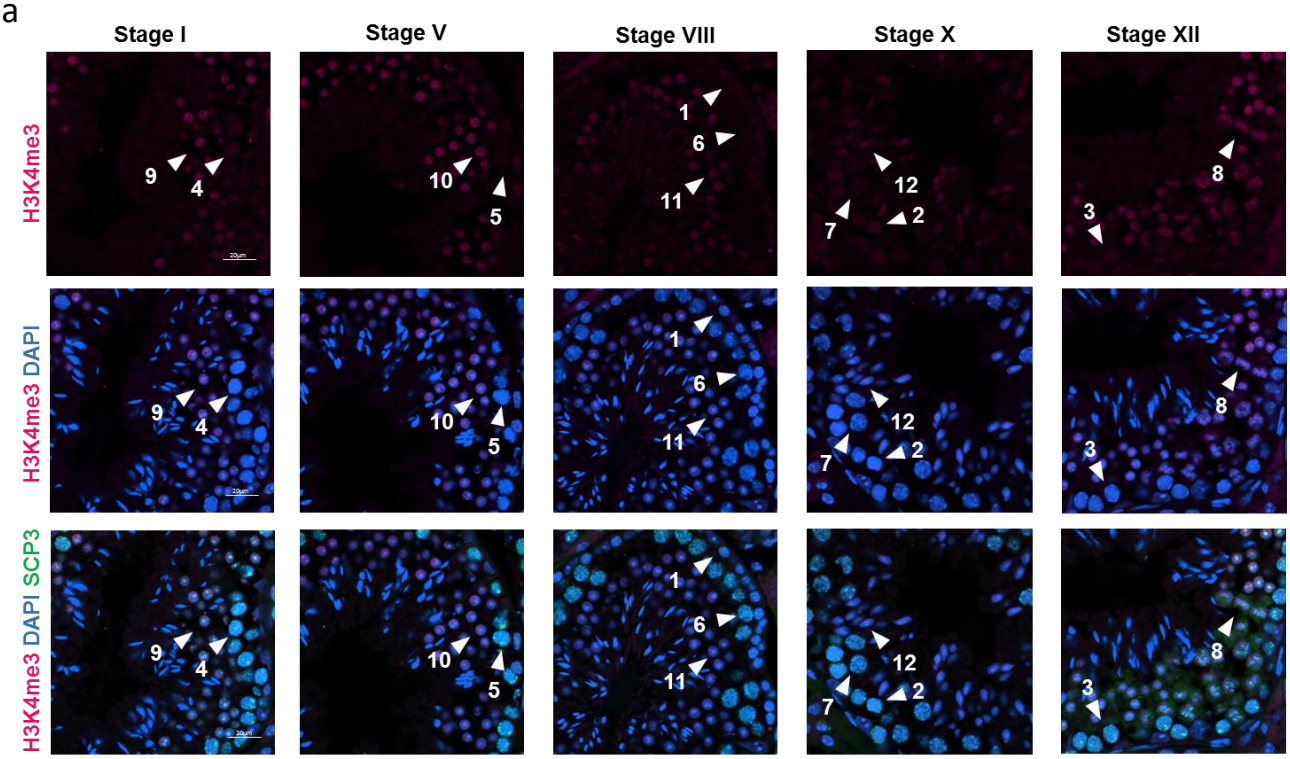

b

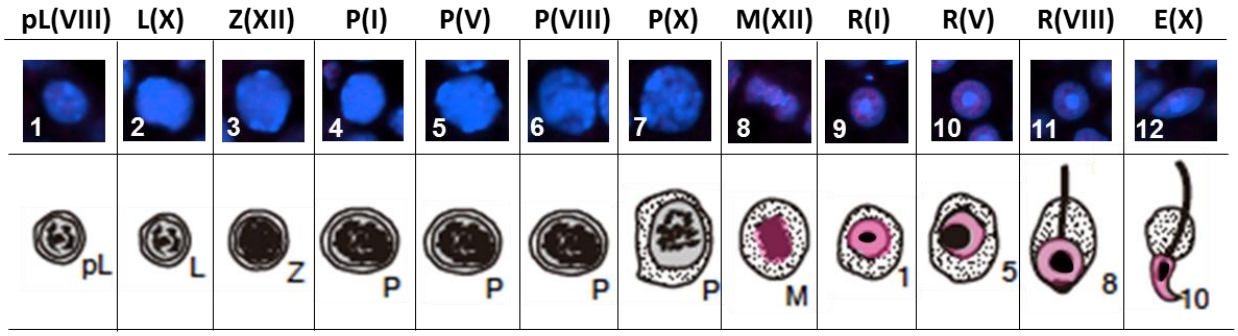

(Modified from Hess & de Franca, 2008)

Fig. 3

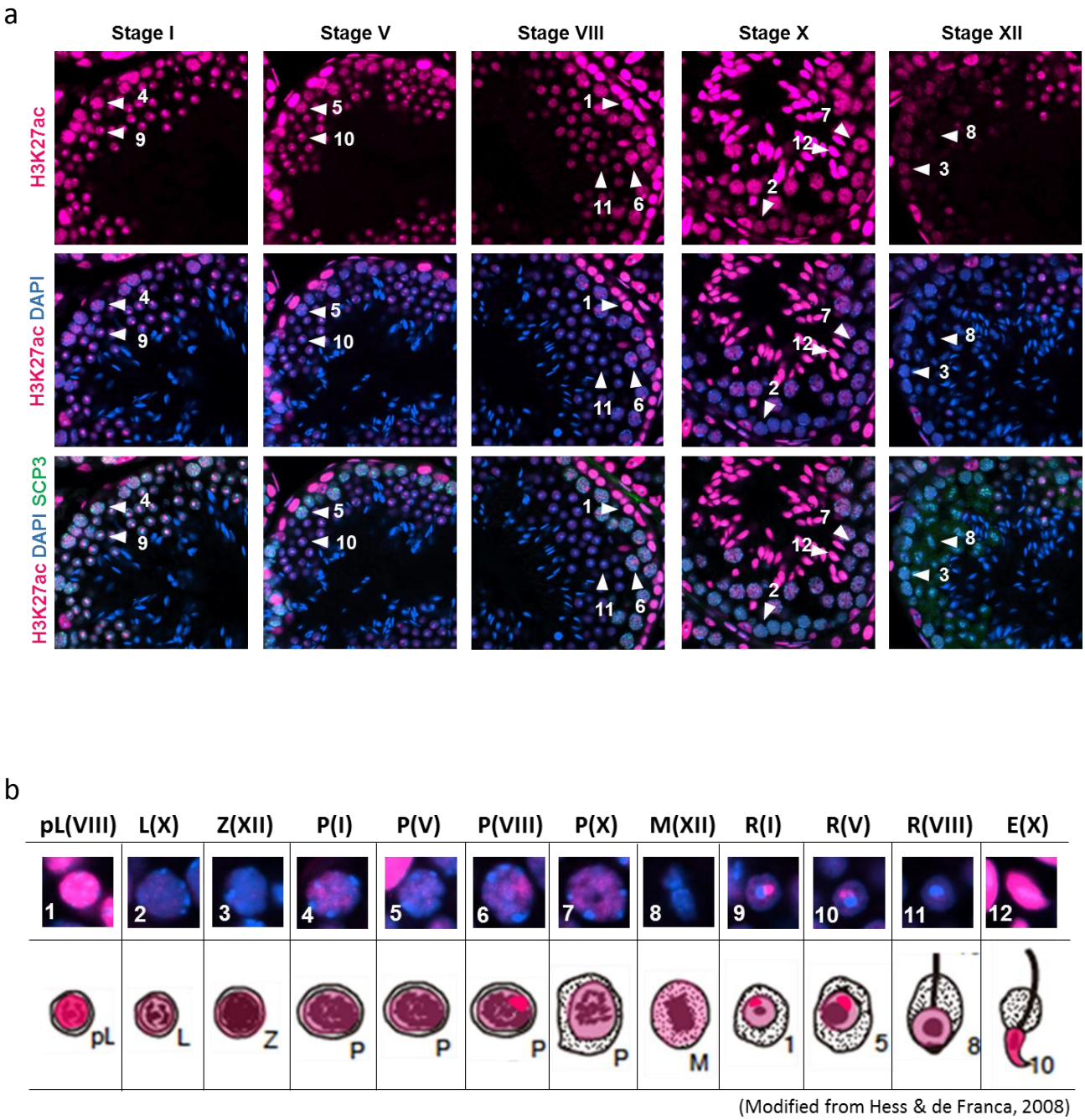
a
Stage I
Stage V
Stage VIII
Stage X
Stage XII
H3K27ac
H3K27ac DAPI
H3K27ac DAPI SCP3
b
pL(VIII)
L(X)
Z(XII)
P(I)
P(V)
P(VIII)
P(X)
M(XII)
R(I)
R(V)
R(VIII)
E(X)
(Modified from Hess & de Franca, 2008)

Fig. 4

a

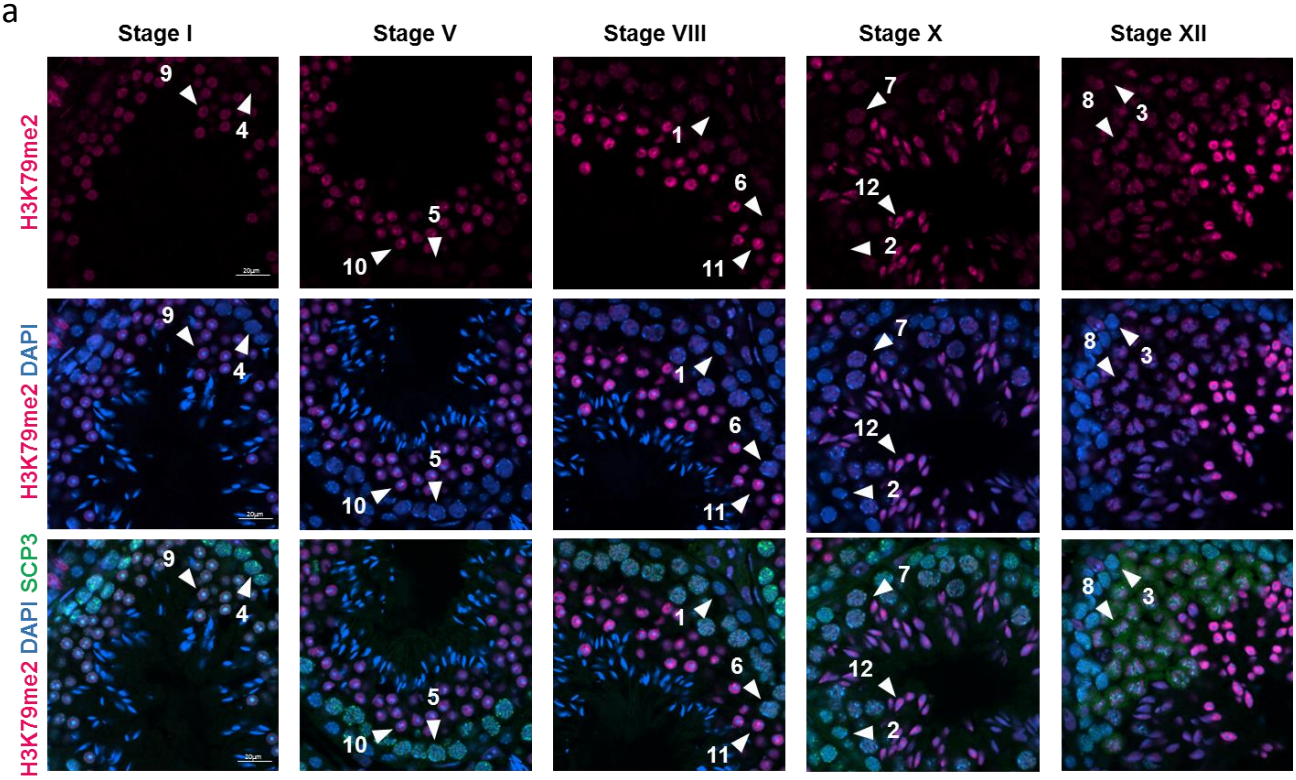

b

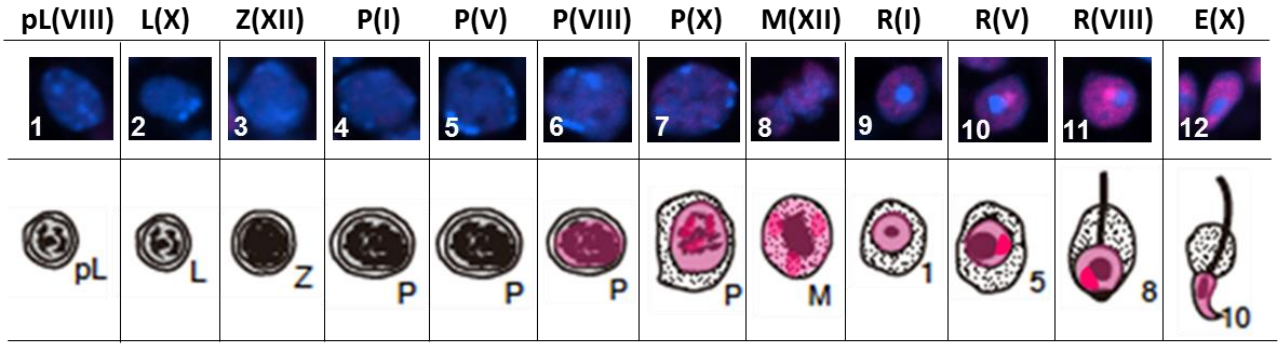

(Modified from Hess & de Franca, 2008)

Fig. 5

a

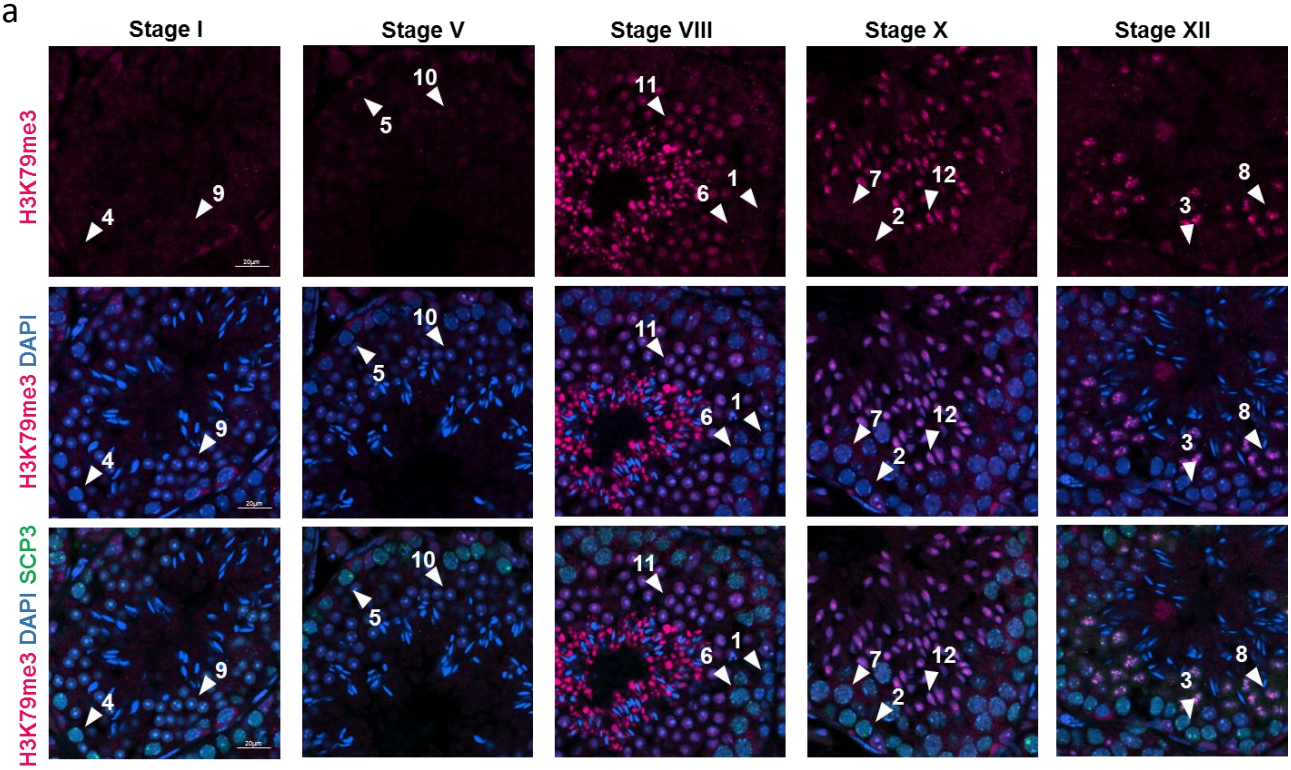

b

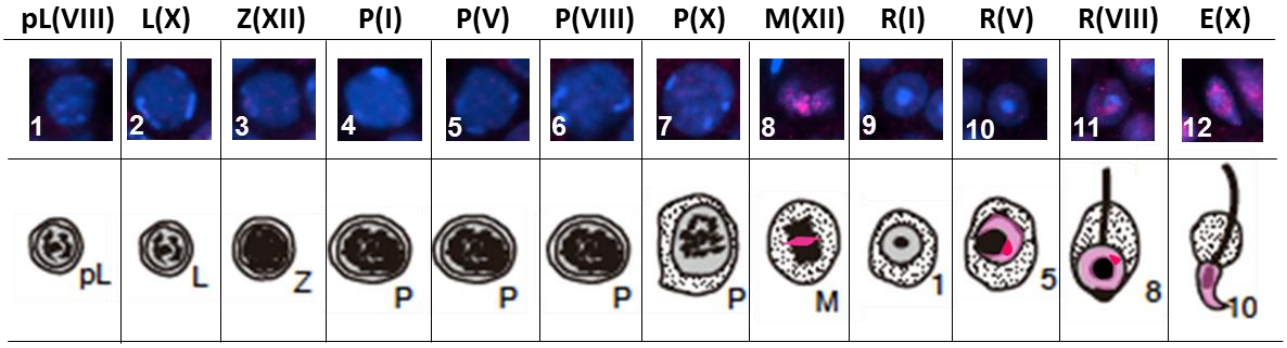

(Modified from Hess & de Franca, 2008)

Fig. 6

a

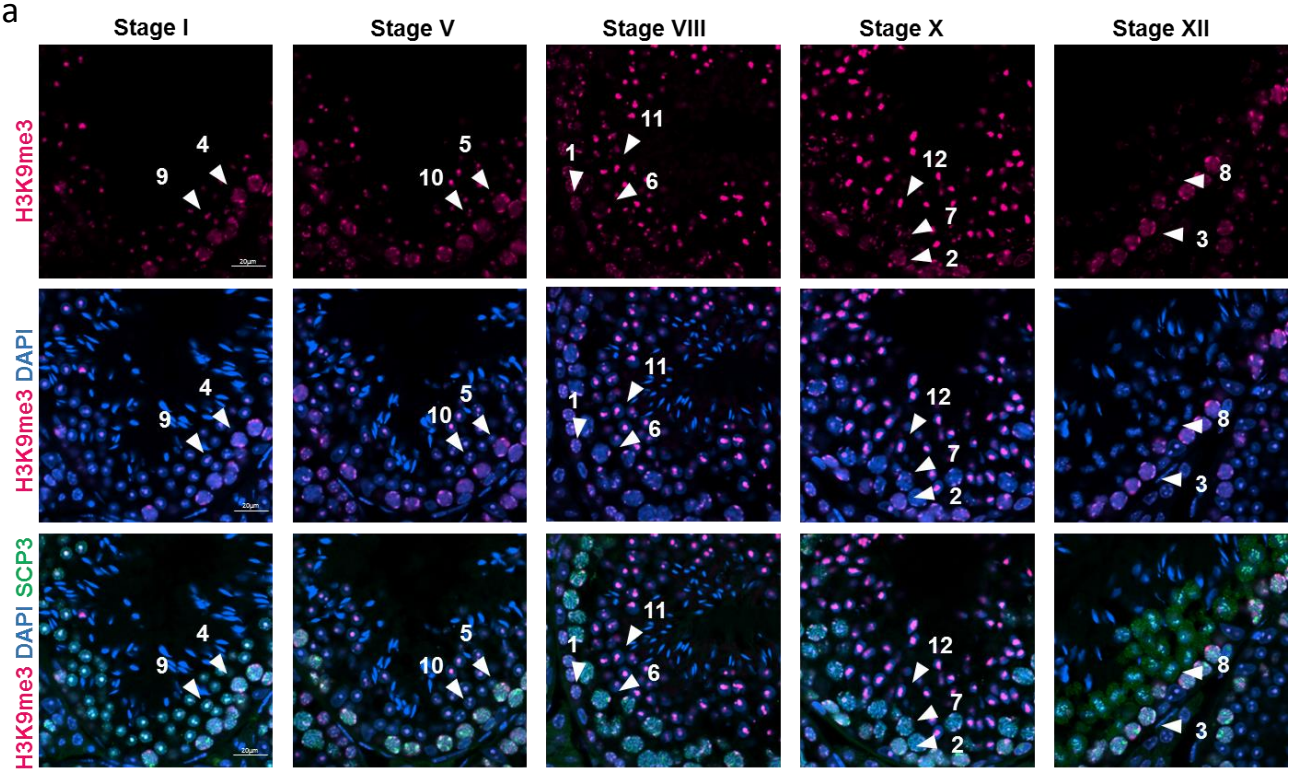

b

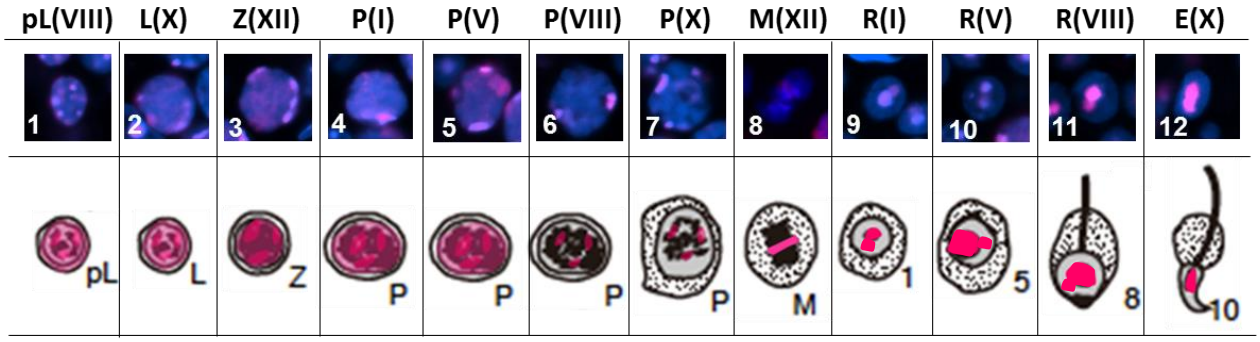

(Modified from Hess & de Franca, 2008)

Fig. 7 a

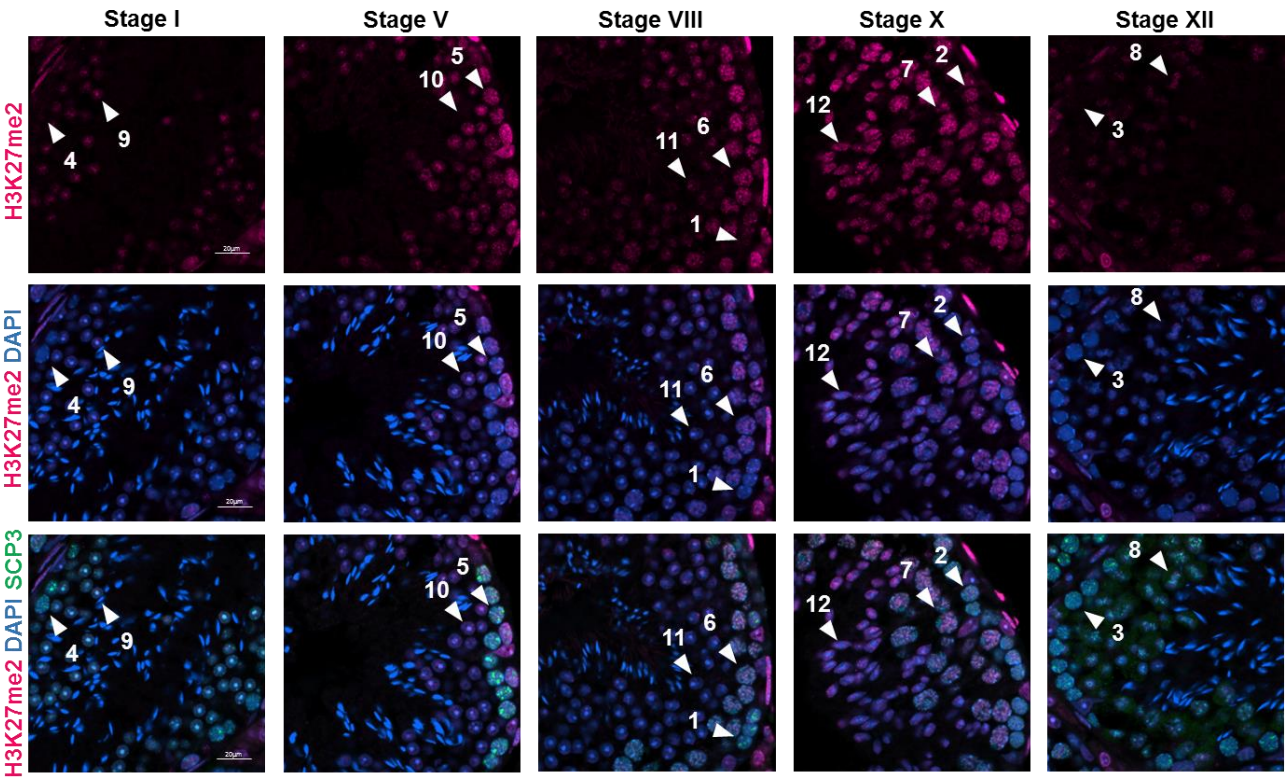

b

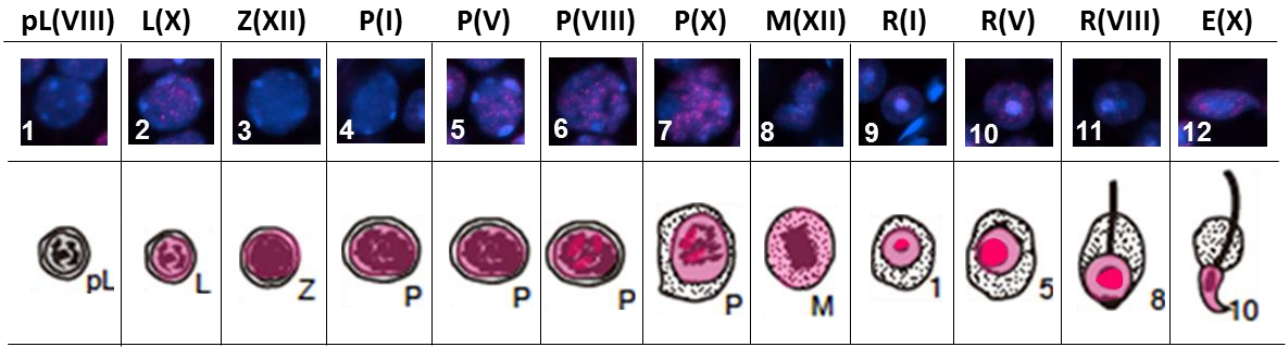

(Modified from Hess & de Franca, 2008)

Fig. 8

a

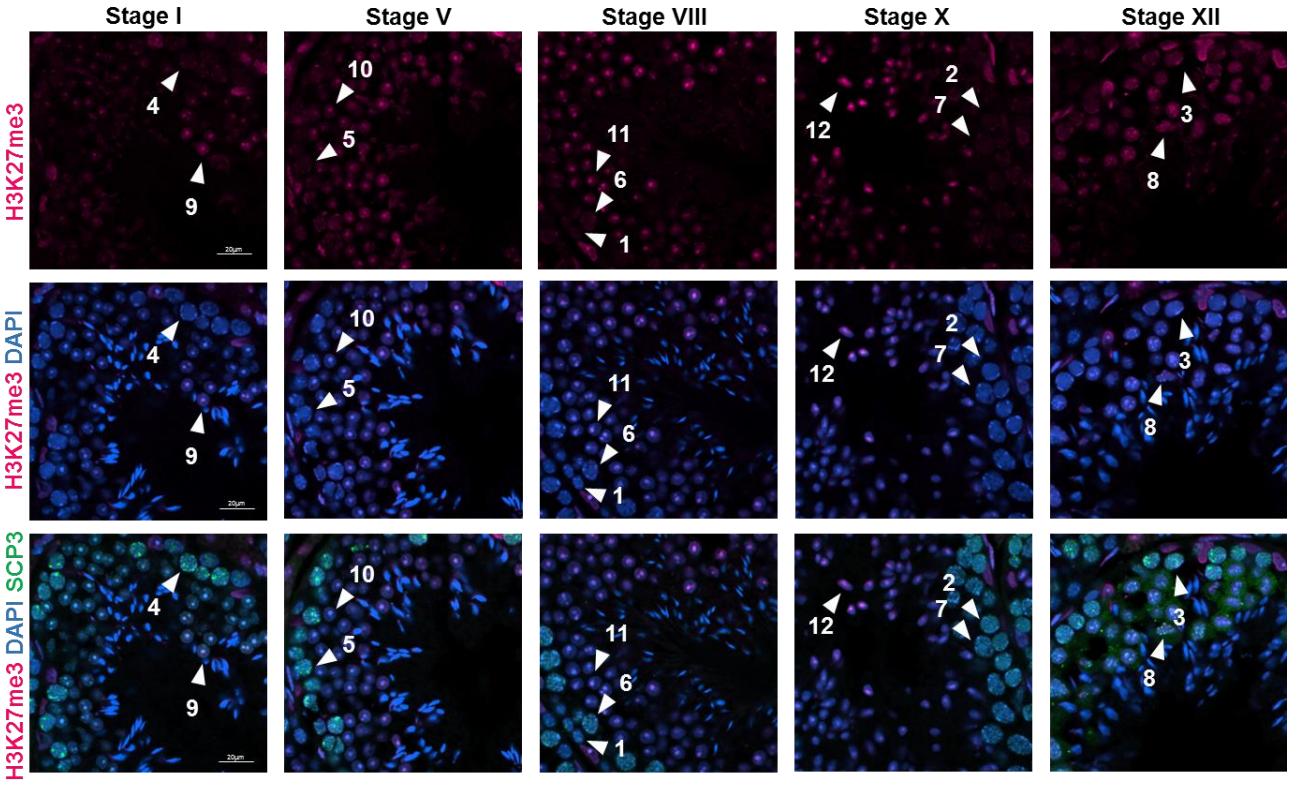

b

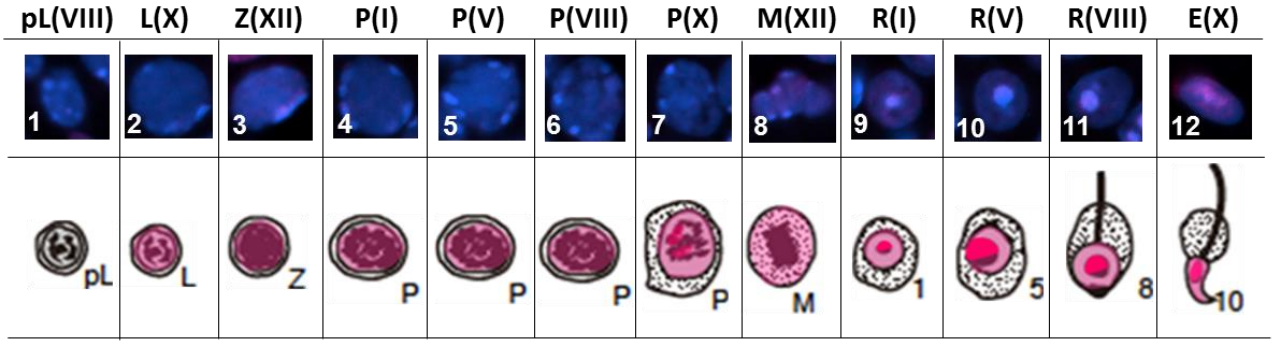

(Modified from Hess & de Franca, 2008)

Fig. 9 a

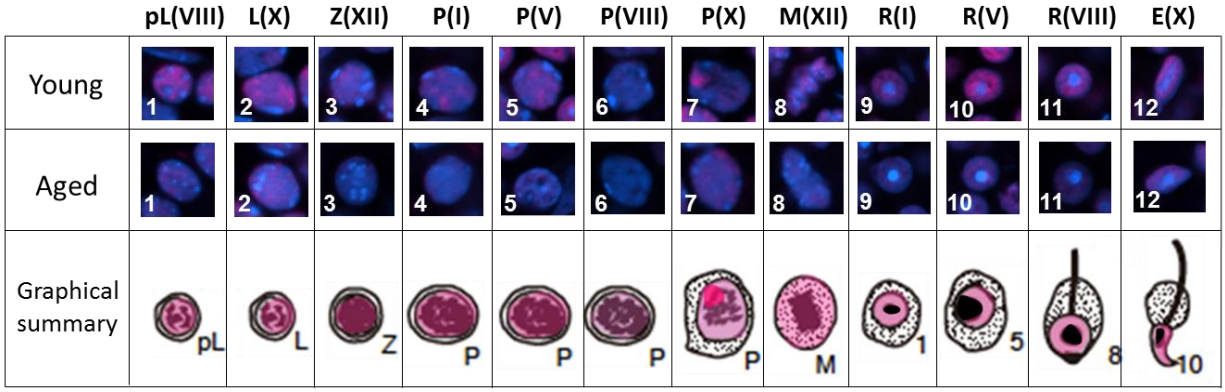

(Modified from Hess & de Franca, 2008)

b

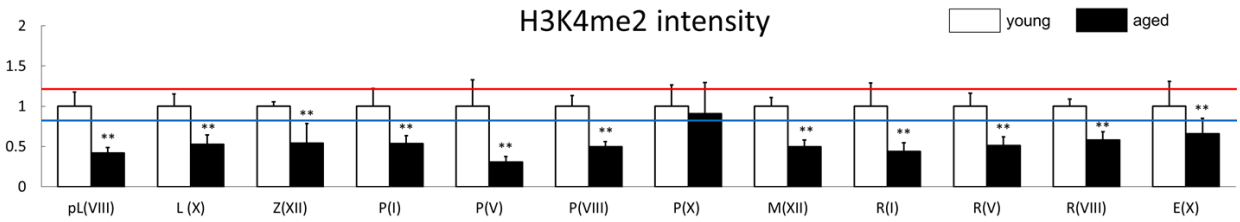

pL: Preleptotene, L: Leptotene, Z: Zygotene, P: Pachytene, M: M phase, R: Round, E: Elongated

Fig. 10 a

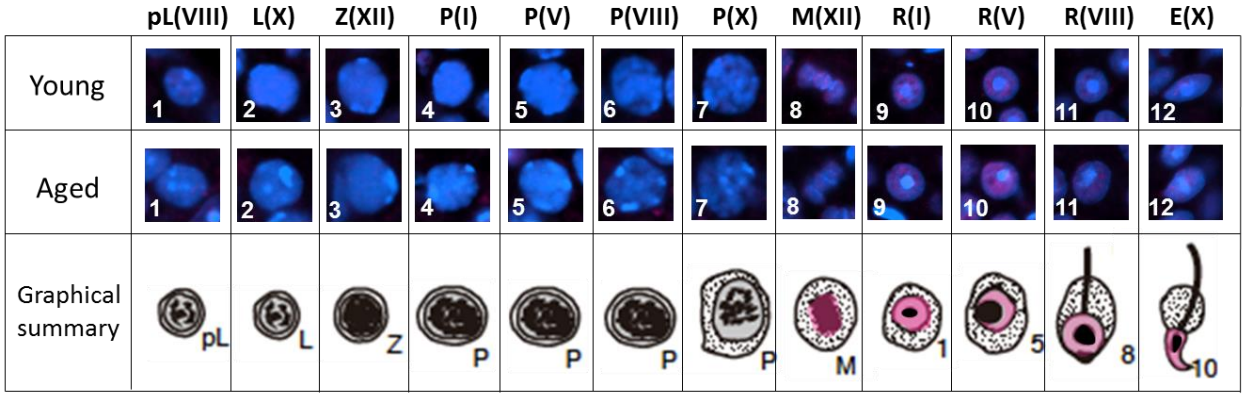

(Modified from Hess & de Franca, 2008)

b

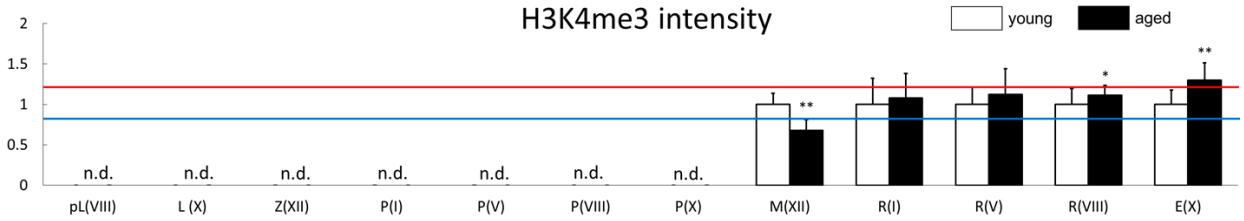

pL: Preleptotene, L: Leptotene, Z: Zygotene, P: Pachytene, M: M phase, R: Round, E: Elongated

Fig. 11 a

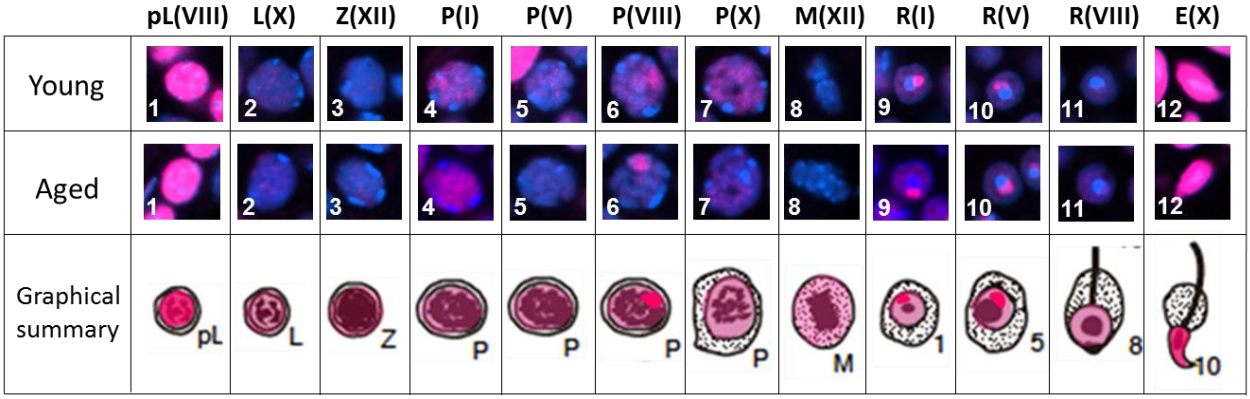

(Modified from Hess & de Franca, 2008)

b

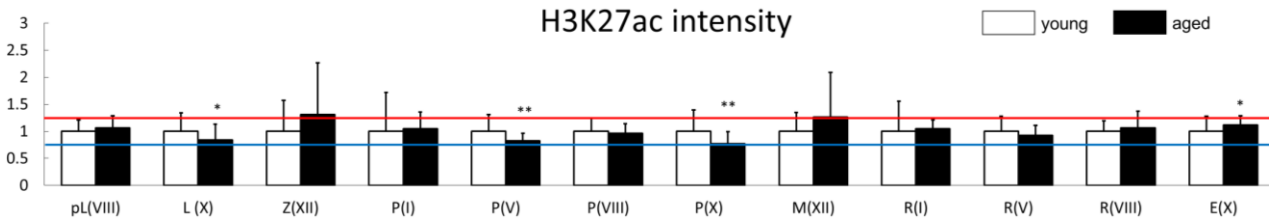

pL: Preleptotene, L: Leptotene, Z: Zygotene, P: Pachytene, M: M phase, R: Round, E: Elongated

Fig. 12 a

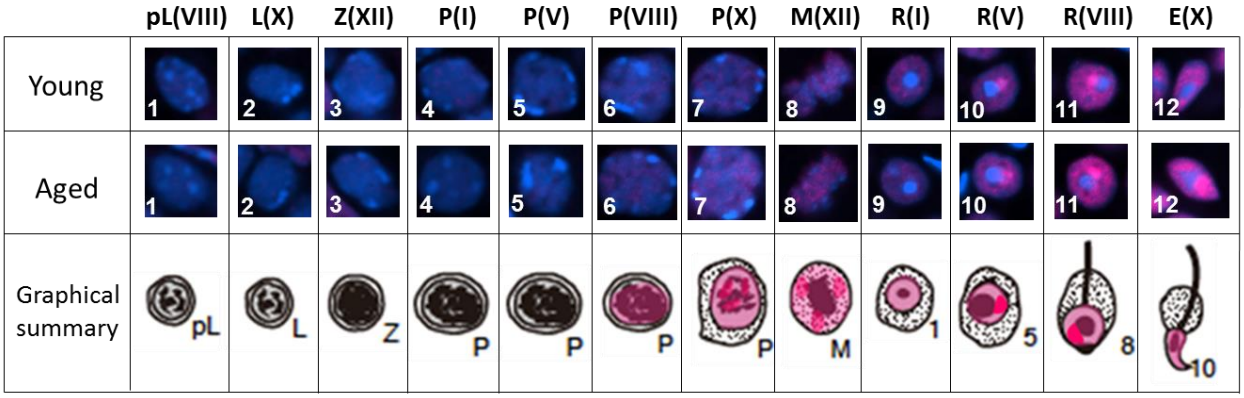

(Modified from Hess & de Franca, 2008)

b

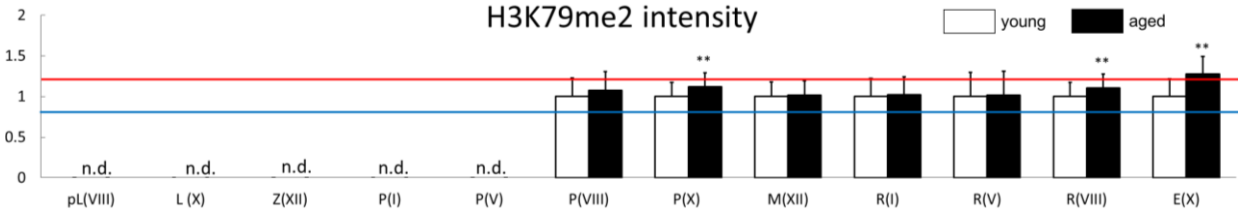

pL: Preleptotene, L: Leptotene, Z: Zygotene, P: Pachytene, M: M phase, R: Round, E: Elongated

Fig. 13 a

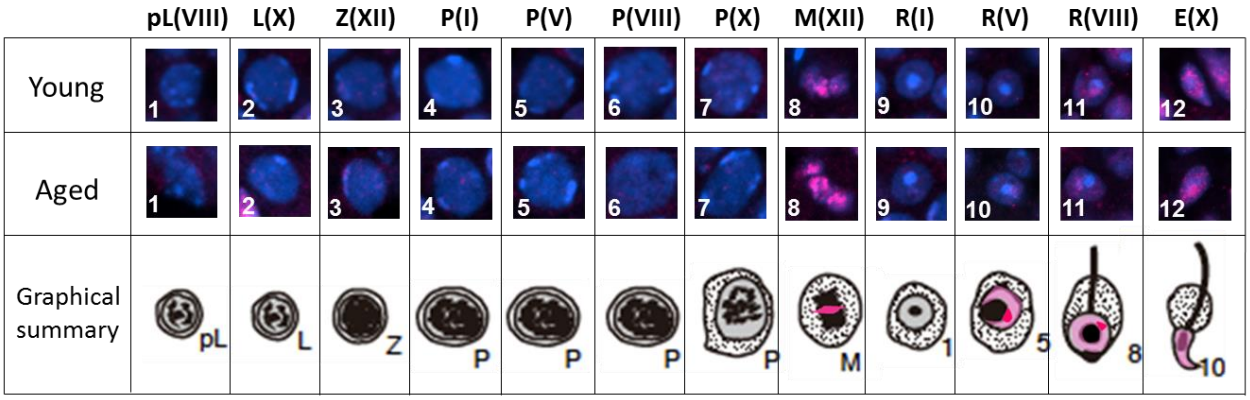

(Modified from Hess & de Franca, 2008)

b

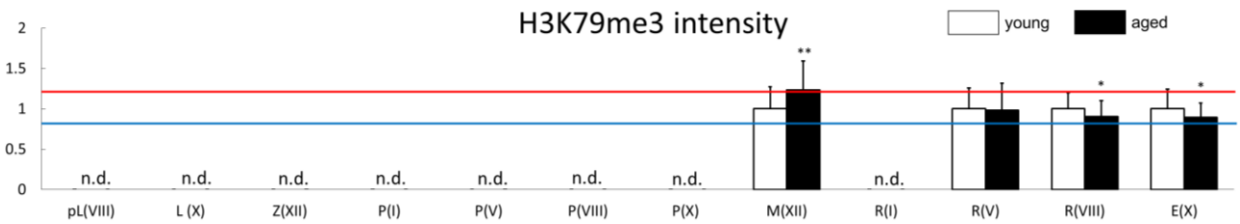

pL: Preleptotene, L: Leptotene, Z: Zygotene, P: Pachytene, M: M phase, R: Round, E: Elongated

Fig. 14 a

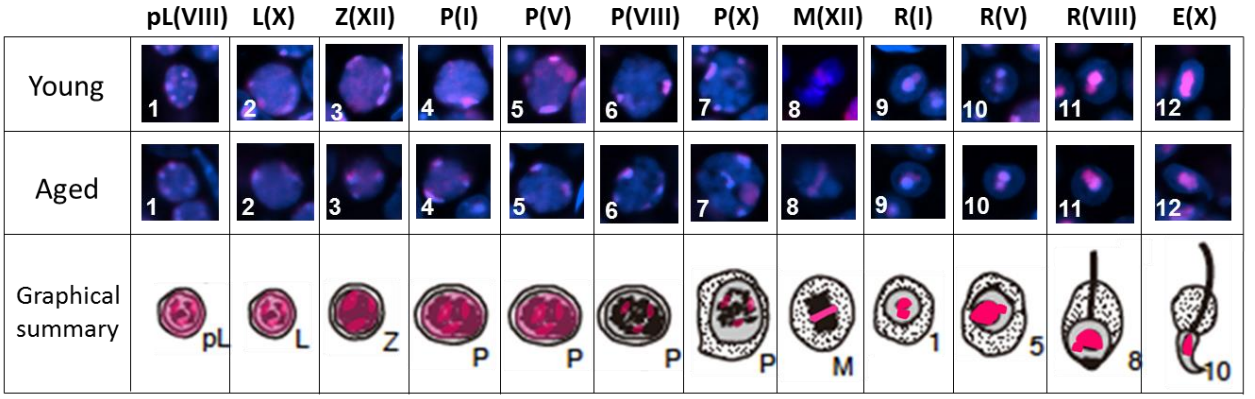

(Modified from Hess & de Franca, 2008)

b

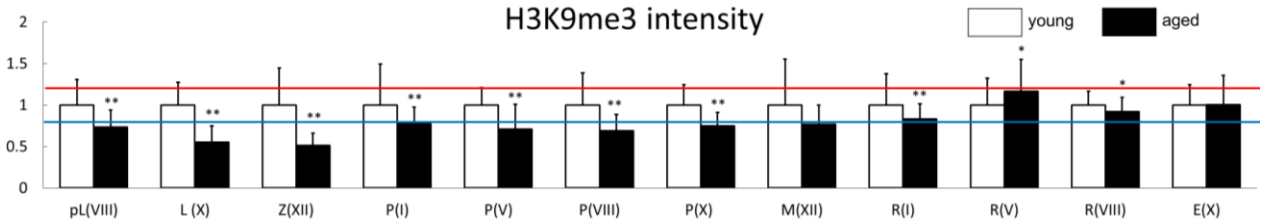

pL: Preleptotene, L: Leptotene, Z: Zygotene, P: Pachytene, M: M phase, R: Round, E: Elongated

Fig. 15 a

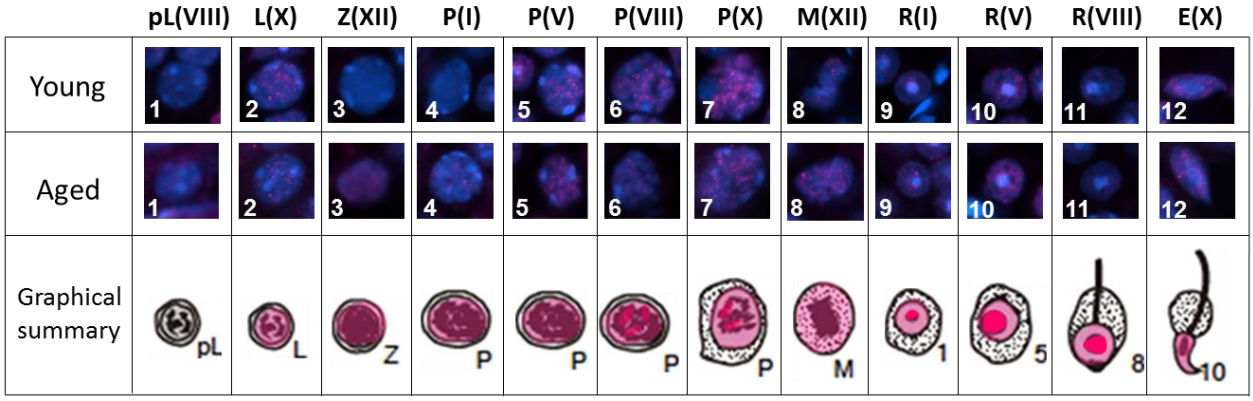

(Modified from Hess & de Franca, 2008)

b

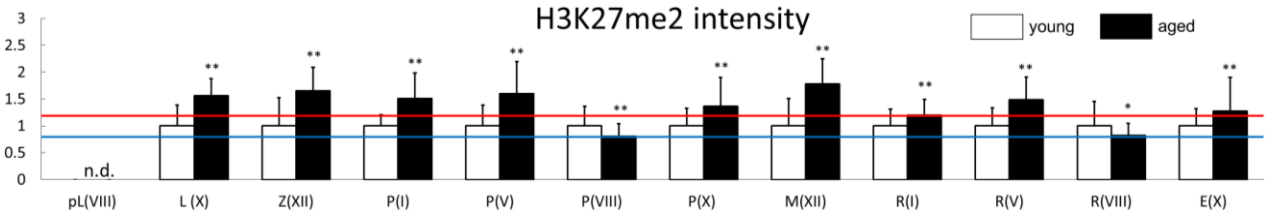

pL: Preleptotene, L: Leptotene, Z: Zygotene, P: Pachytene, M: M phase, R: Round, E: Elongated

Fig. 16 a

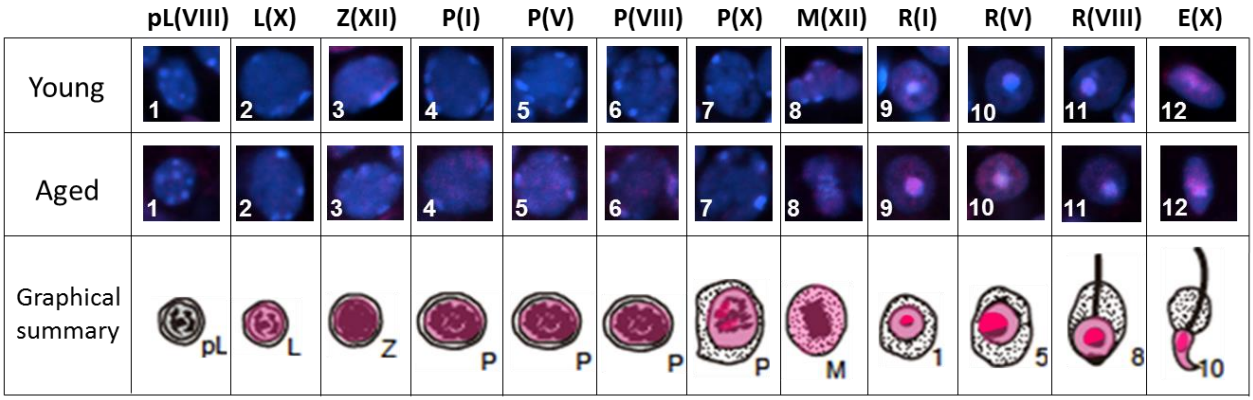

(Modified from Hess & de Franca, 2008)

b

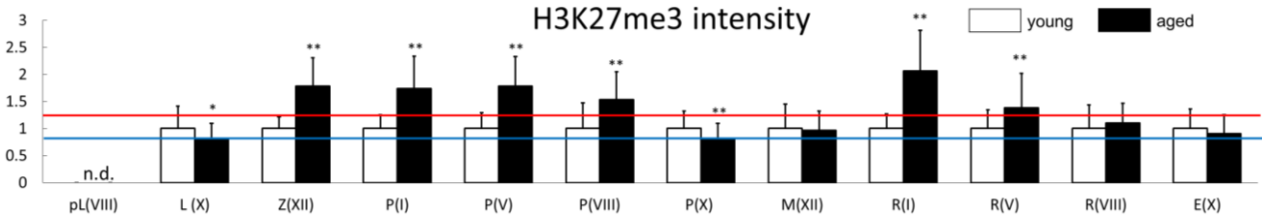

pL: Preleptotene, L: Leptotene, Z: Zygotene, P: Pachytene, M: M phase, R: Round, E: Elongated

Fig. 17 a

pL
L
Z
P
P
P
P
M
1
5
8
10

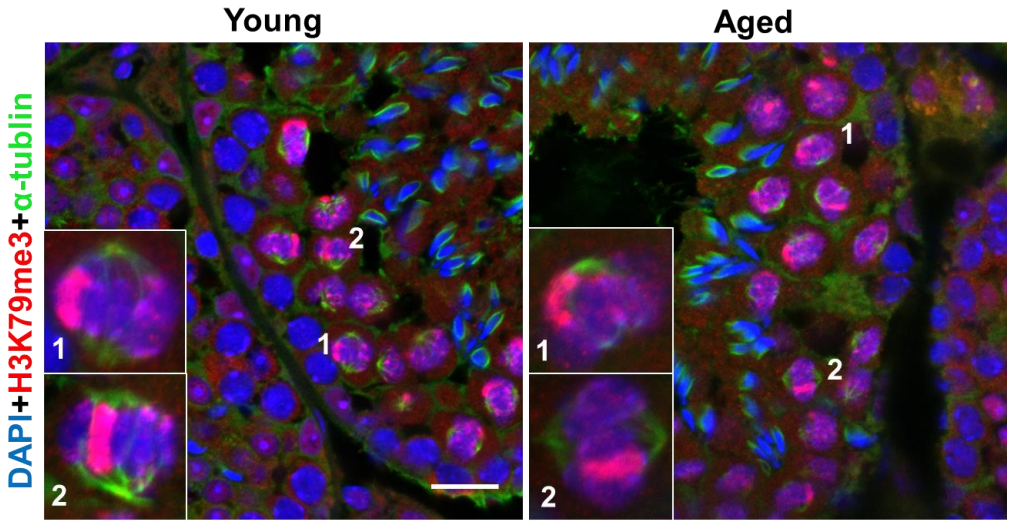
Young
Aged
DAPI+H3K79me3+α-tublin
1
2
1
2
1
2
1
2

b

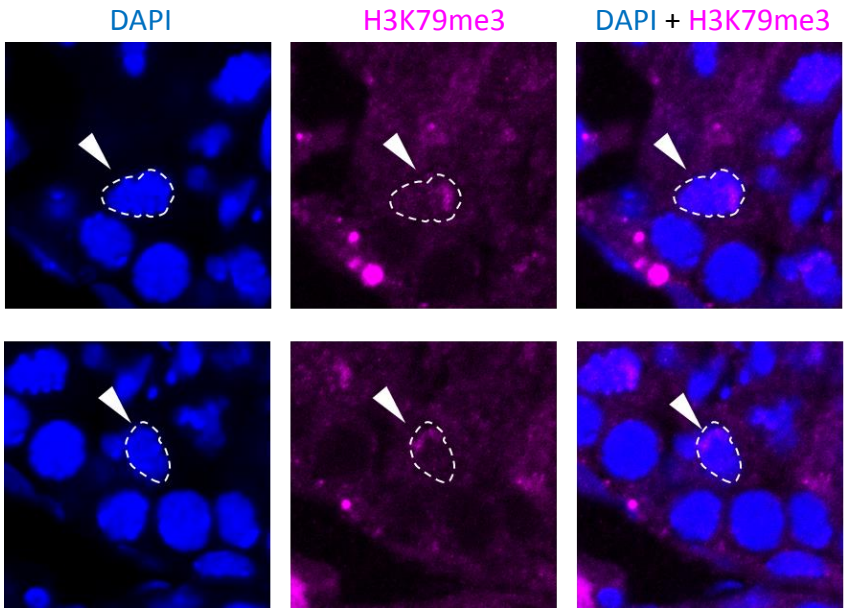
DAPI
H3K79me3
DAPI + H3K79me3

c

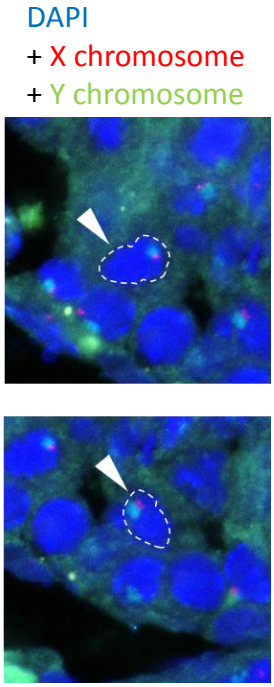
DAPI
+ X chromosome
+ Y chromosome